Cenozoic stratigraphy and subsidence history of the South China Sea margin in the Taiwan region

A. T. Lin,*[1] A. B. Watts† and S. P. Hesselbo†

*Department of Earth Sciences, National Central University, Chungli, Taiwan
†Department of Earth Sciences, University of Oxford, Parks Road, Oxford OX1 3PR, UK

ABSTRACT

Seismic reflection profiles and well data are used to determine the Cenozoic stratigraphic and tectonic development of the northern margin of the South China Sea. In the Taiwan region, this margin evolved from a Palaeogene rift to a latest Miocene–Recent foreland basin. This evolution is related to the opening of the South China Sea and its subsequent partial closure by the Taiwan orogeny.

Seismic data, together with the subsidence analysis of deep wells, show that during rifting ($\sim$58–37 Ma), lithospheric extension occurred simultaneously in discrete rift belts. These belts form a $>$200 km wide rift zone and are associated with a stretching factor, β, in the range $\sim$1.4–1.6. By $\sim$37 Ma, the focus of rifting shifted to the present-day continent–ocean boundary off southern Taiwan, which led to continental rupture and initial seafloor spreading of the South China Sea at $\sim$30 Ma. Intense rifting during the rift–drift transition ($\sim$37–30 Ma) may have induced a transient, small-scale mantle convection beneath the rift. The coeval crustal uplift (Oligocene uplift) of the previously rifted margin, which led to erosion and development of the breakup unconformity, was most likely caused by the induced convection.

Oligocene uplift was followed by rapid, early post-breakup subsidence ($\sim$30–18 Ma) possibly as the inferred induced convection abated following initial seafloor spreading. Rapid subsidence of the inner margin is interpreted as thermally controlled subsidence, whereas rapid subsidence in the outer shelf of the outer margin was accompanied by fault activity during the interval $\sim$30–21 Ma. This extension in the outer margin ($\beta\sim$1.5) is manifested in the Tainan Basin, which formed on top of the deeply eroded Mesozoic basement. During the interval $\sim$21–12.5 Ma, the entire margin experienced broad thermal subsidence. It was not until $\sim$12.5 Ma that rifting resumed, being especially active in the Tainan Basin ($\beta\sim$1.1). Rifting ceased at $\sim$6.5 Ma due to the orogeny caused by the overthrusting of the Luzon volcanic arc.

The Taiwan orogeny created a foreland basin by loading and flexing the underlying rifted margin. The foreland flexure inherited the mechanical and thermal properties of the underlying rifted margin, thereby dividing the basin into north and south segments. The north segment developed on a lithosphere where the major rift/thermal event occurred $\sim$58–30 Ma, and this segment shows minor normal faulting related to lithospheric flexure. In contrast, the south segment developed on a lithosphere, which experienced two more recent rift/thermal events during $\sim$30–21 and $\sim$12.5–6.5 Ma. The basal foreland surface of the south segment is highly faulted, especially along the previous northern rifted flank, thereby creating a deeper foreland flexure that trends obliquely to the strike of the orogen.
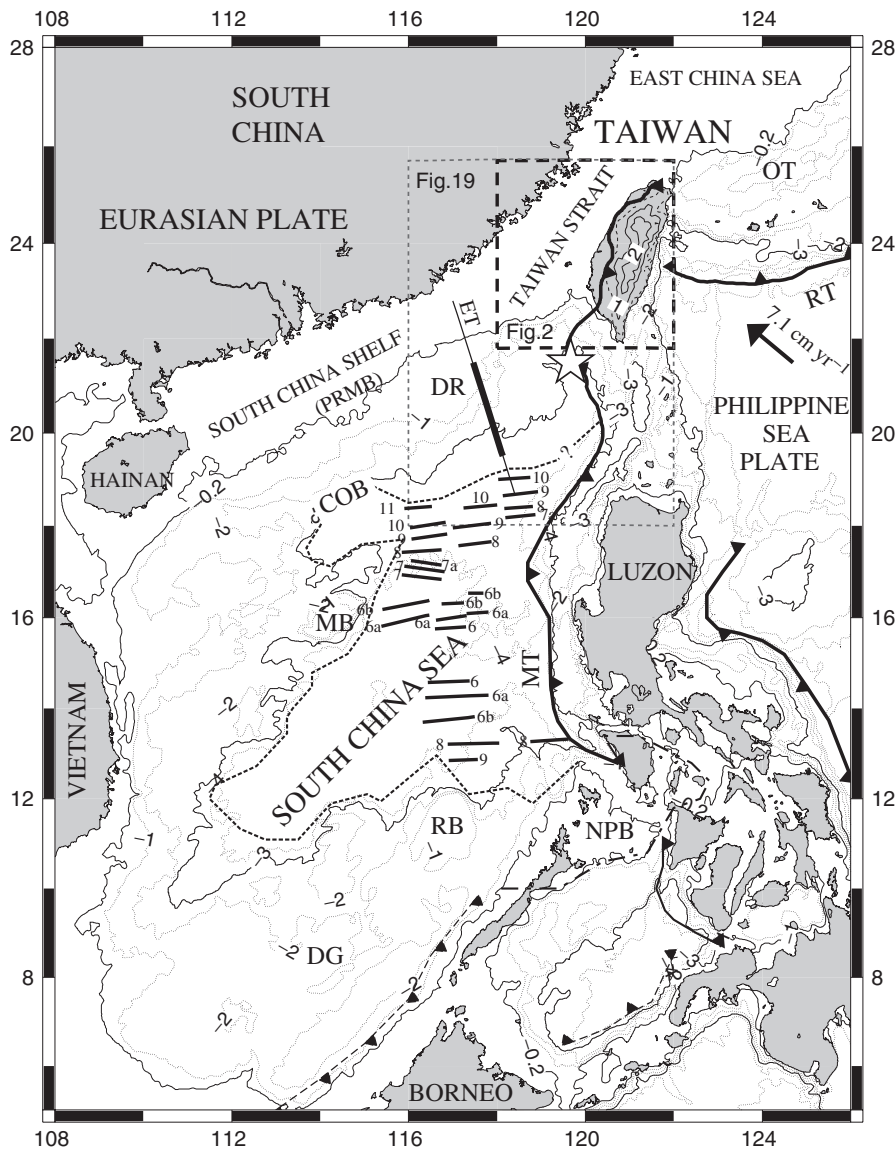
INTRODUCTION

The Taiwan region (Fig. 1) in the present day comprises an orogenic belt that has overthrust the northern margin of the South China Sea (Teng, 1990). This margin has re-

Correspondence: A. T. Lin, Department of Earth Sciences, National Central University, Chungli, Taiwan. E-mail: lin@earth.ncu.edu.tw
[1] Formerly of the Department of Earth Sciences, University of Oxford.

corded a complete Wilson cycle that begins with the formation of an adjacent ocean basin (i.e. the South China Sea) by continental breakup and ends with subsequent oceanic closure by collision (i.e. the Luzon arc–south China margin collision). This evolutionary cycle was achieved within just $\sim$58 Myr and the collisional processes are still active.

A large quantity of seismic reflection and borehole data have been collected in the Taiwan region during the past 30 years in order to establish a framework for petroleum exploration. These data have been used in previous studies

Fig. 1. Bathymetry and tectonic framework in and around the South China Sea. The thick line in the northern margin of the South China Sea across the Dongsha Rise (DR) and along the eastern transect (ET) reported in Nissen *et al.* (1995a) shows the position of the high-velocity (7.0–7.5 km s^{-1}) lower crustal layer. The star off SW Taiwan shows the location of thick extrusive rocks reported in Sibuet *et al.* (2002). The ages for the seafloor magnetic anomalies (bold lines, Cl1 to C5, Taylor & Hayes (1983); Briais *et al.* (1993)) of the South China Sea are shown in Fig. 14. Water depths are shown in kilometres. The 0.2- and 3-km isobaths are plotted as solid lines and other isobaths are shown as dotted lines for a 1-km contour interval. The topography (in km) on the Taiwan island is shown for 0.2 (dashed line), 1 and 2 km contours (solid lines), respectively. COB = continent–ocean boundary, DG = Dangerous Grounds, DR = Dongsha Rise, MB = Macclesfield Bank, MT = Manila Trench, NPB = North Palawan block, OT = Okinawa Trough, RB = Reed Bank, RT = Ryukyu Trench.
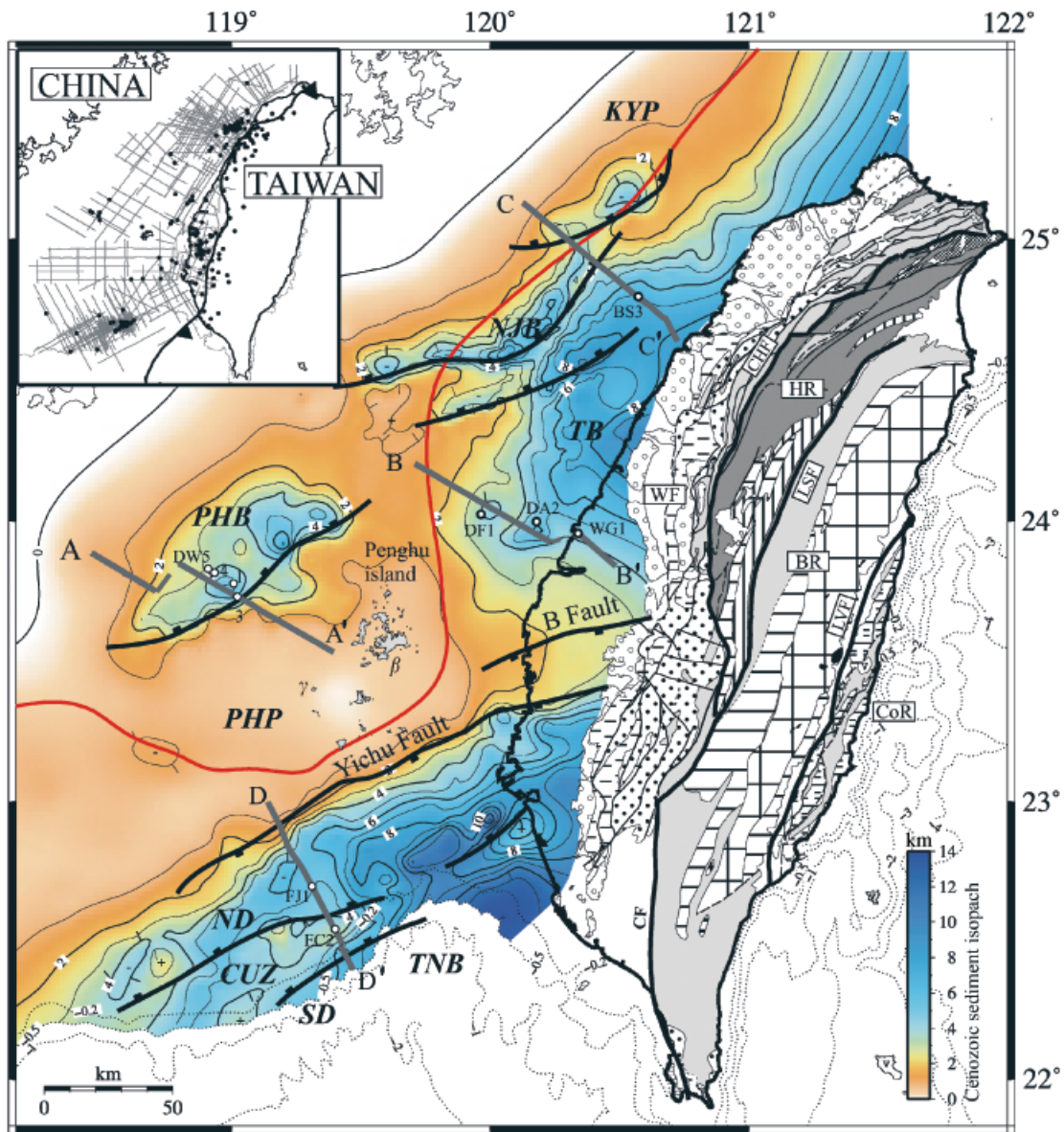
to either schematically outline the regional basin framework (e.g. Sun, 1982) or to determine the tectonic development of individual basins and platforms; for example, the Taihsi Basin (e.g. Huang *et al.*, 1993; Shen *et al.*, 1996), Tainan Basin (e.g. Yang *et al.*, 1991; Lee *et al.*, 1993b; Tzeng *et al.*, 1996), Penghu Basin (e.g. Hsiao *et al.*, 1991), Nanjihtao Basin (e.g. Chow *et al.*, 1991) and the Penghu Platform (e.g. Tang, 1977). The purpose of this paper is to determine the Cenozoic stratigraphy and tectonic development of the Taiwan region using seismic reflection and borehole data (inset figure in Fig. 2). To this end, well-log sequence correlation, backstripping and tectono-stratigraphic sequence mapping have been applied to the subsurface data set. This analysis reveals the spatial and temporal tectonic development of the Taiwan region, from syn-rift through post-breakup into foreland basin development. We argue that some of the 'anomalous' features of the margin, such as the margin-scale uplift associated with the formation of the breakup unconformity, vigorous volcanism, anomalously rapid early post-breakup subsidence and post-breakup extensions, can be accounted

for by induced mantle convection during the rift–drift transition.

GEOLOGICAL SETTING

The South China Sea (Fig. 1) is bounded in the north by the passive south China continental margin (Taylor & Hayes, 1980, 1983). To the south, small continental blocks that were rifted off mainland Asia, i.e. the terrains of North Palawan (NPB), Reed Bank (RB) and other shoal areas (Dangerous Grounds, DG), separate the basin from an extinct subduction zone along Palawan and northwest Borneo (Holloway, 1982; Taylor & Hayes, 1983). To the east, a westerly moving Luzon arc–trench system, the leading edge of the Philippine Sea plate, borders the South China Sea basin, with its northernmost segment over-riding the South China Sea margin in the Taiwan sector.

The South China Sea is associated with seafloor-spreading-type magnetic anomalies Cl1 to C5C, suggesting an age of 30–16 Ma for the basin (Taylor & Hayes, 1980, 1983). (Note

Fig. 2. Geological framework of the Taiwan region. The Cenozoic sediment isopach (in km) shows the superimposed development of a foreland basin on top of a rifted margin. The present-day foreland basin is delimited by the Taiwan orogen in the east and the eastern boundary of the foreland forebulge in the west (the red line along the middle of the Taiwan Strait). The inset figure shows the subsurface data set used in this study. The geology of the Taiwan orogen is according to Ho (1986) and the bathymetry (in km) is shown as dashed lines. Seismic reflection profiles AA′ to DD′ are shown in Figs 5–8, respectively. West Taiwan basins/highs: CUZ = Central Uplift Zone, KYP = Kuanyin Platform, ND = Northern Depression, NJB = Nanjihtao Basin, PHB = Penghu Basin, PHP = Penghu Platform, SD = Southern Depression, TNB = Tainan Basin, TB = Taihsi Basin. Taiwan orogen: BR = Backbone Range, CoR = Coastal Range, HR = Hsuehshan Range, WF = Western Foothills. Major faults: CF = Chaochou, CHF = Chuchih, LSF = Lishan, LVF = Longitudinal Valley.

that the magneto-chronology is based on Cande & Kent (1995).) On the basis of the magnetic lineation pattern, Lee & Lawver (1992, 1994) restored the positions of southward drifted terranes back to anomaly C11 time (mid-Oligocene) and placed the Reed Bank and North Palawan blocks up against the China margin near SW Taiwan.

Overthrusting of the Luzon arc on the northern South China Sea margin since the late Miocene (Teng, 1990) has exhumed material that was previously located in the outer part of the rifted margin (Figs 2 and 3). The Taiwan orogenic belt presently comprises four geological provinces. From east to west, they are the Coastal Range (CoR), Backbone Range (BR), Hsuehshan Range (HR) and Western Foothills (WF) (Ho, 1986). The terrains are of Eurasian plate affinity, with the exception of the Coastal Range, which incorporates the accreted volcanic arc and belongs to the Philippine Sea plate. The Backbone Range and Hsuehshan Range are collectively referred to as the Central Range, which comprises the main body of the Taiwan orogen. The Central Range consists of pre-Tertiary continental basement unconformably overlain by metamorphosed Eocene to Miocene clastics deposited during the Palaeogene rifting and Oligocene–Miocene post-breakup phases. The WF province is a west-vergent, fold-and-thrust belt comprising an Oligocene–Pleistocene siliciclastic sequence that accumulated on a passive margin and, subsequently, in a foreland basin setting.

To the west of the orogen, the rifted margin structures are overlain by a foreland basin sequence in the regions of the Taiwan Strait and western Coastal Plain (Figs 2 and 3). A Cenozoic succession, up to 10 km thick in places, floored with a block-faulted pre-Tertiary basement, underlies this region.

Figure 4 summarises the Cenozoic stratigraphy in the Taiwan region. The figure shows that three major unconformities (the late Palaeocene rift-onset, early Oligocene breakup and latest Miocene basal foreland) bound tectono-stratigraphic units deposited during the three stages of syn-rift, post-breakup and foreland basin.

Four basins separated by basement highs can be recognised from the Cenozoic sediment isopach map (Fig. 2). These are the Nanjihtao (NJB), Penghu (PHB), Taihsi (TB) and Tainan (TNB) Basins (Sun, 1982). The Penghu (Fig. 5) and Nanjihtao (Fig. 7) Basins, situated on the inner shelf, are two *en echelon*, NE-trending half-grabens and are bounded by normal faults to the SE (Sun, 1982). Both basins feature a tilted Palaeogene rift-graben structure that is truncated by flat-lying Miocene post-rift sediments. The inner basins are either situated on the present-day foreland forebulge, such as the Penghu Basin, or are partially buried by a distal foreland basin sequence, such as the Nanjihtao Basin (Figs 2 and 3b and d). The Taihsi (Figs 6 and 7) and Tainan (Fig. 8) Basins are separated by a basement high – the Penghu Platform (PHP) (Fig. 2). The Taihsi Basin features a broadly subsided region deepening eastwards and bounded by the Kuanyin Platform (KYP) and the Penghu Platform to the north and south, respectively. It shows three phases of superimposed basin development: from bottom to top, Palaeogene rift, Oligo-cene–Miocene post-breakup and latest Miocene–Recent foreland basin (Figs 2 and 3a–c).

To the south of the Penghu Platform, a series of short E–W trending normal faults (Yang *et al.*, 1991) downthrow to the south and border the Tainan Basin. These E–W trending normal faults are shown, for simplicity, as one continuous boundary fault, the Yichu Fault (Fig. 2). Unlike the rest of the neighbouring basins, the Tainan Basin is largely devoid of the Palaeogene syn-rift sediments (Lee *et al.*, 1993b). Instead, boreholes in the basin only recovered Oligocene–Recent strata overlying Mesozoic basement, and these record the post-breakup and foreland basin development phases.

The Kuanyin Platform in the north and the Penghu Platform in the south are two 'stable' areas and were relatively sediment-free during the Cenozoic. These two shallow-basement highs preserve thin Miocene post-breakup sediments draping the Mesozoic basement that now underlies an eastward deepening foreland basin.

STRATIGRAPHIC DEVELOPMENT

The first stage of this study was to determine the stratigraphic development of the Taiwan region using about 200 boreholes and ∼20 000 line-km seismic reflection profiles (Fig. 2). To this end, we correlate the three major unconformities (i.e. rift-onset, breakup and basal foreland) in the study area using the subsurface data set. The results are a series of time–structure maps for the major unconformable surfaces. The time–structure maps were then converted to depth maps using velocity information from about 23 well check-shot surveys (Lin, 2001). Additionally, the Oligocene–Miocene post-breakup succession was divided into 16 well-log stratigraphic sequences as detailed in Lin (2001). The main results of these correlations and interpretations are a series of isopach maps showing the spatial distribution of sediments accumulated during the Palaeogene syn-rift (Fig. 9), Oligocene–Miocene post-breakup (Figs 10 and 17) and the latest Miocene–Recent foreland basin (Fig. 11). This section summarises the stratigraphic development in the Taiwan region as it evolved from rifting to orogenic loading.

Palaeocene–Eocene syn-rift episode (∼58–37 Ma)

Pre-rift strata and the rift-onset unconformity

The Mesozoic pre-rift strata consist of continental to shallow-marine deposits. The rift-onset unconformity (ROU in Figs 5–7) marks the inception of the Palaeogene rift episode and separates the syn-rift strata from the underlying pre-rift Mesozoic sedimentary (or basement) rocks (Fig. 4). According to the well data, the oldest sediments that lie above this unconformity are of late Palaeocene age (i.e. zone NP5 at THS1 well (Huang & Chi, 1979)), whereas the age of the sediments underlying the unconformity is generally early Cretaceous (Aptian) (Huang, 1978). Hence, the rift-onset unconformity may represent a missing stratigraphic section
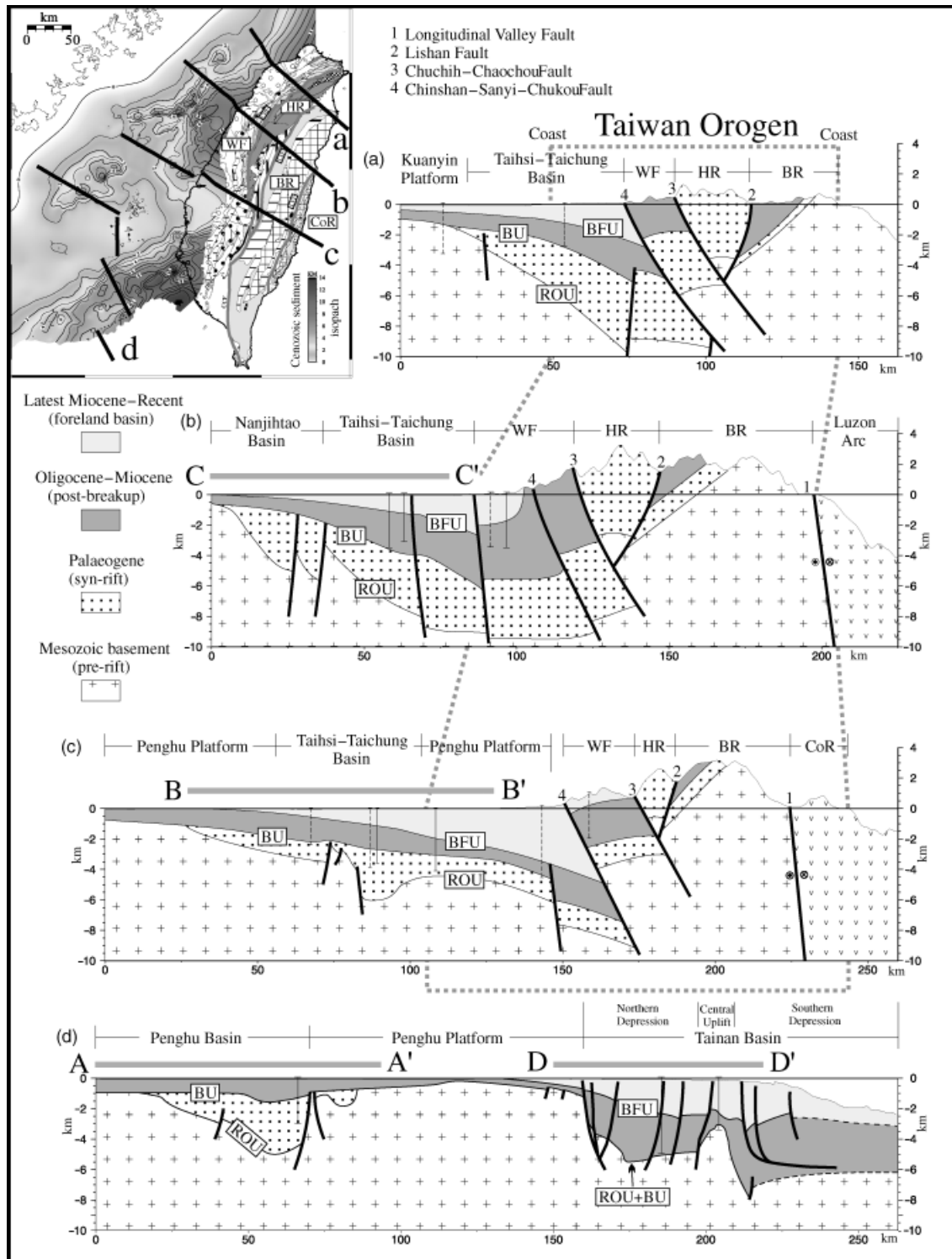
Fig. 3. Profiles showing the upper crustal structures across the northern margin of the South China Sea in the Taiwan region. The profiles in offshore regions are from depth-converted seismic sections and the structures beneath the Taiwan orogen are schematic plots. Some of the seismic sections (AA′ to DD′) used for constructing the upper crustal structure are shown in Figs 5–8. The inset figure shows the locations of the profiles. ROU = rift-onset unconformity, BU = breakup unconformity, BFU = basal-foreland unconformity. Other abbreviations are as in Fig. 2.

of upper Cretaceous to lower Palaeocene (about 110–60 Ma) representing a duration of ∼ 50 Myr.

The equivalent rift-onset unconformity has been exposed by late Cenozoic orogenic processes in the Back-bone Range, onshore Taiwan, where an unconformity separates the pre-Cenozoic basement rocks, or the Tananao Complex, from the overlying Pilushan Formation of Eocene age (Figs 2 and 4).
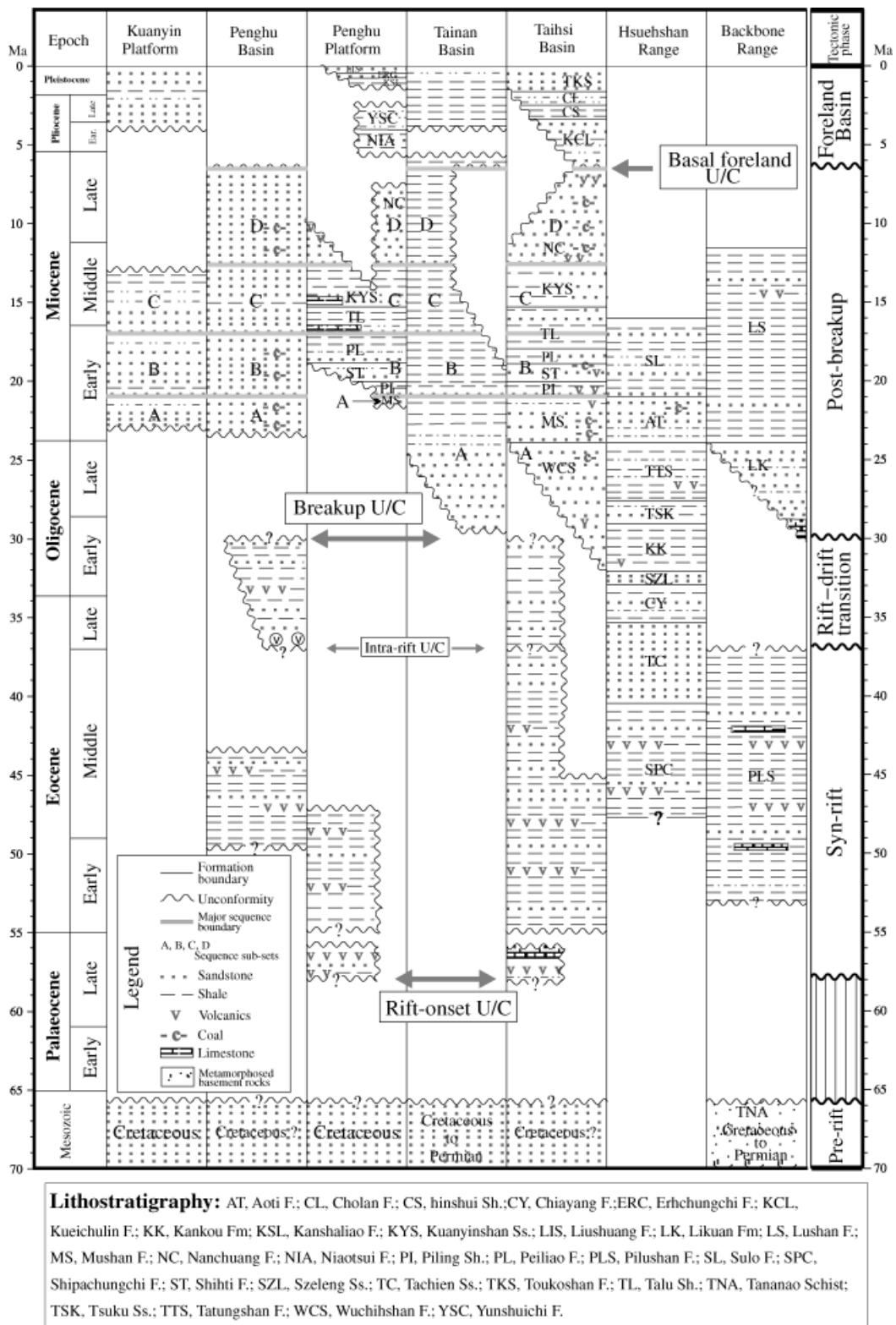
Fig. 4. Cenozoic stratigraphy (sources: this study; Huang, 1982; Ho, 1986) and tectonic phases in the Taiwan region suggested in this study. The post-breakup succession is further divided into four (A, B, C and D) sequence sets. U/C = unconformity.

Syn-rift tectonic development

The Palaeogene syn-rift strata are bracketed by unconformities of the late Palaeocene rift-onset at their base and

Oligocene breakup at their top. On the basis of drilling evidence, the syn-rift sequence is dominantly shale intercalated with few sandstone beds and volcanic rocks, laid down in shallow-marine to continental environments as
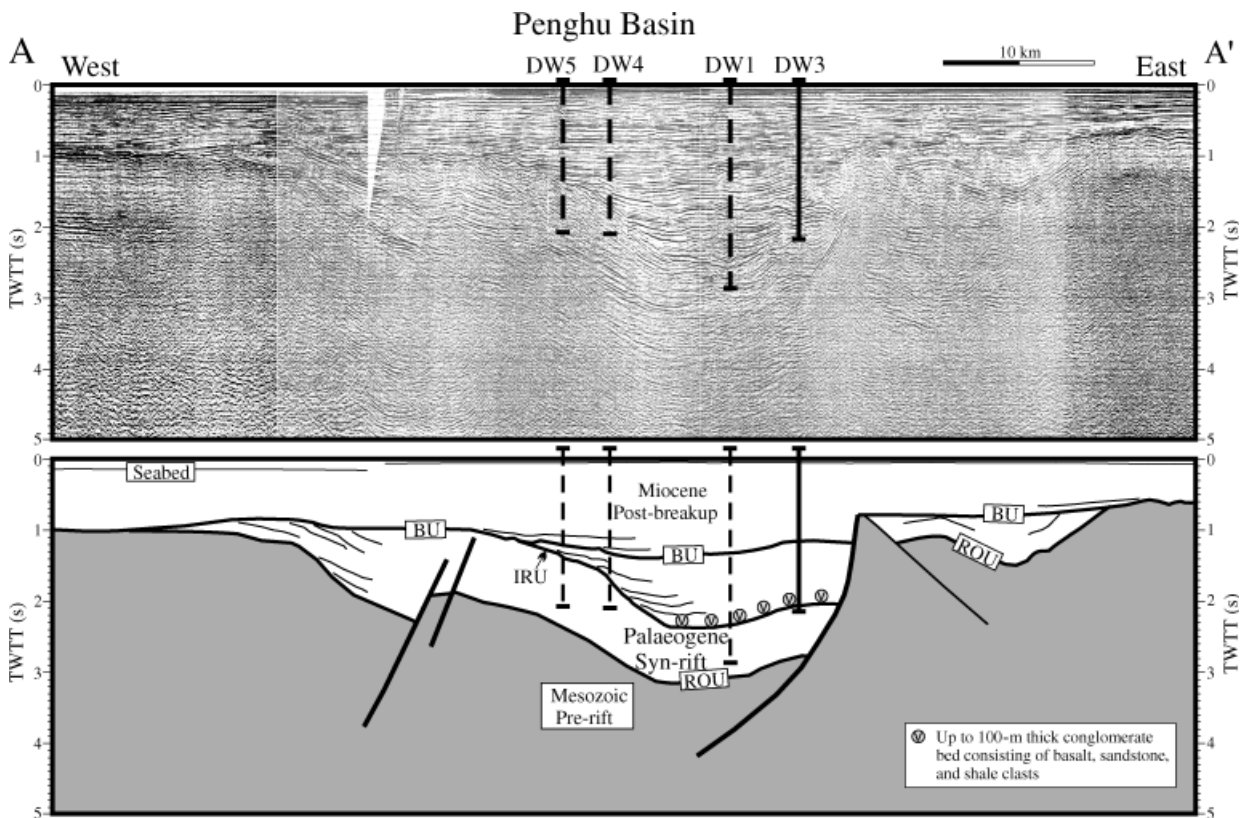
Fig. 5. Seismic section AA′ (see Fig. 2 for location) across the Penghu Basin. Note (1) the absence of crustal tilting toward the Taiwan orogen in the east and (2) the development of intra-rift unconformity (IRU) and a local sedimentary wedge on top of the Palaeogene syn-rift strata.

judged from fossils content. The syn-rift succession accumulated in the fault-bounded Nanjihtao, Penghu, Taihsi and Tainan Basins in the west offshore basins (Fig. 9).

In the Penghu Basin (Fig. 5) and southern Taihsi Basin (Fig. 6), there is a local, angular unconformity termed 'intra-rift unconformity' (IRU) in the syn-rift succession, which appears to be truncated by the later breakup unconformity. The development of this local unconformity is interpreted to mark the end of Palaeogene rifting and the onset of regional crustal uplift and erosion at ~ 37 Ma prior to continental breakup at ~ 30 Ma (Lin, 2001). The isopach map for the pre-breakup strata (Fig. 9) was prepared by subtracting the depth structure map of the breakup unconformity from that of the rift-onset unconformity. Up to 5 km of pre-breakup strata accumulated in the Nanjihtao, Penghu and Taihsi Basins. In addition, thin Palaeogene sediments are also present in the Penghu Platform and the northern Tainan Basin, but the syn-rift sequence there is not mapped in this study because of uncertainty in defining its base.

Equivalent Palaeogene sediments have also been exposed by later collisional processes in the Backbone and Hsuehshan Ranges (Figs 2, 4 and 9). The exposed lithology is similar to the subsurface equivalent in the west. In the Backbone Range, the age of this syn-rift sequence is mainly early–middle Eocene (~ 53–40 Ma, NP12–NP16) as determined from studies on nannofossil biostratigraphy (Huang, 1980a, b). The age of the lowermost syn-rift deposits is unknown, however, due to the lack of age-diagnostic

fossils. The earliest syn-rift sediments in the Backbone Range are therefore at least early Eocene (NP12) age, i.e. > 53 Ma, and probably older (late Palaeocene?).

In summary, extension occurred more or less simultaneously in the Taiwan region during late Palaeocene at discrete loci. The rift centres include the Nanjihtao, Penghu and Taihsi Basins, as well as the more distal rift setting that is now exposed in the Backbone Range. A few shallow rift structures also developed in the Penghu Platform and, possibly, in the northern Tainan Basin. This rift zone is at least > 200 km in width from the inner rift basins (the Nanjihtao and Penghu Basins) to the Backbone Range. The age of initial rifting is taken to be, in this study, the base of zone NP6 (58 Ma) in the late Palaeocene, which is about 1 Myr younger than the oldest syn-rift sediments (NP5) that lie directly on the Mesozoic basement and were found at THS1 well on the Penghu Platform (Huang & Chi, 1979). Syn-rift sedimentation is accompanied by volcanism. The volcanic activity was also dated to occur during the period ~ 57–38 Ma according to Lo *et al.* (2000).

Oligocene–Miocene post-breakup episode (~ 30–6.5 Ma)

Breakup unconformity (~ 37–30 Ma)

The Oligocene breakup unconformity (BU in Figs 5–8), the most pronounced unconformity in the Taiwan region,
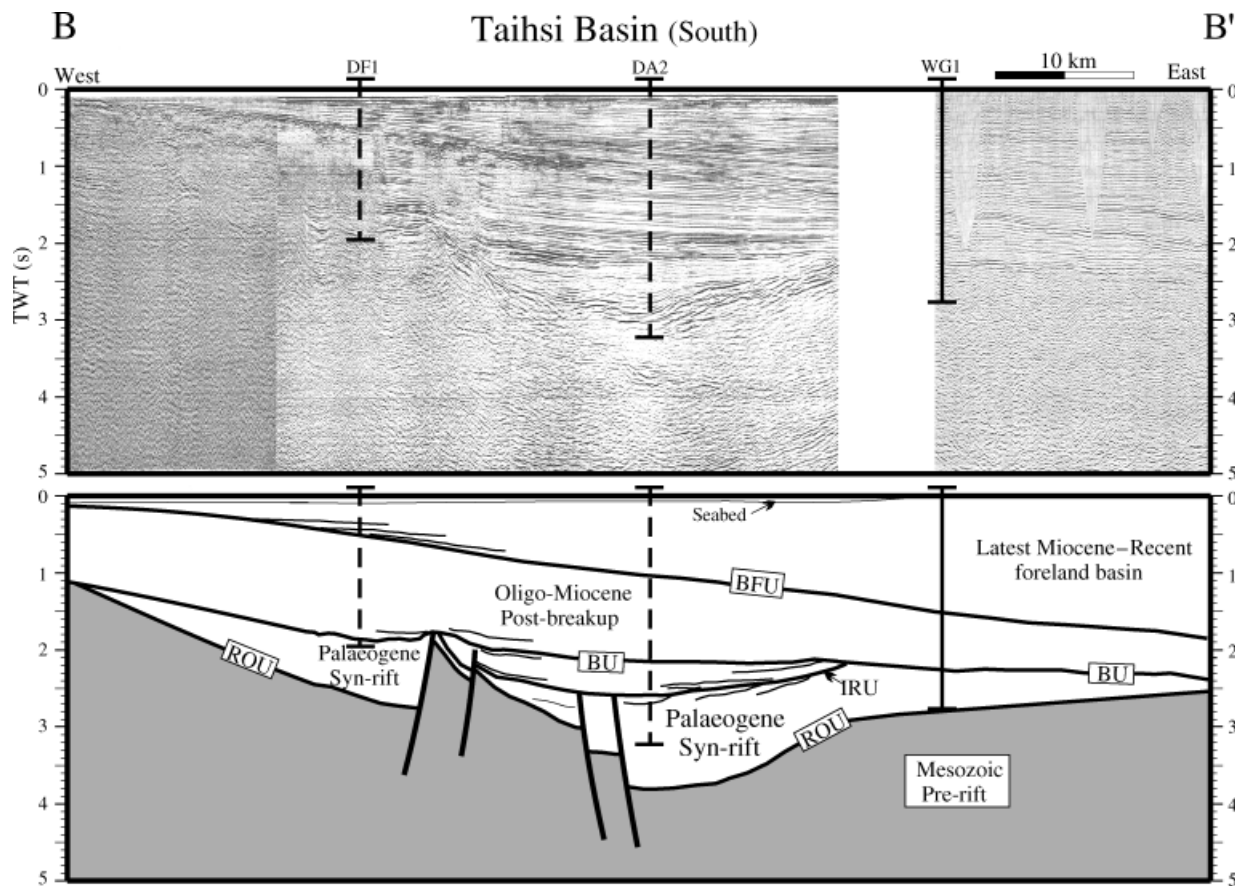
Fig. 6. Seismic section BB′ (see Fig. 2 for location) showing block-faulted Palaeogene structures overlain by a cover of Oligocene–Miocene post-breakup sediments, which is then flexed downwards by the Taiwan orogen in the east. The flexure has caused a basal foreland unconformity (BFU), which separates an onlapping foreland basin sequence above it from passive margin sequences below it. Note the notable onlapping feature of the basal foreland unconformity and the presence of a local intra-rift unconformity (IRU) at the top of the Palaeogene syn-rift sequence.

is present in all regions on the Eurasian plate around Taiwan, with the exception of the Hsuehshan Range, where relatively continuous Oligocene sedimentation has been suggested (e.g. Teng *et al.*, 1991). The unconformity separates the underlying Palaeogene syn-rift strata from the post-breakup sequence and marks the inception of seafloor spreading in the South China Sea at 30 Ma (see below).

In the syn-rift depocentres, the breakup unconformity is characterised by a pronounced stratigraphic gap and strong lithological contrasts across the unconformity. In the rift centre of the northern Taihsi Basin, for example, the breakup unconformity brings upper Oligocene (NP25) sandstone hundreds of metres thick into contact with middle Eocene (NP17) shale (Huang, 1982).

The age of the first sediments overlying the Oligocene breakup unconformity shows a progressively younger age from the outer (i.e. mid-Oligocene, ∼ 30 Ma at the base of zone NP24 in the Tainan Basin) toward the inner margin (i.e. early Miocene, ∼ 23 Ma at the base of NN2 in the Penghu Basin). Strata lying directly beneath the Oligocene breakup unconformity span from late Palaeocene in the rift shoulders to middle Eocene in the rift depocentres. The

Oligocene breakup unconformity therefore represents a missing section ranging at least 37–30 Ma as judged by the ages of its youngest underlying and oldest overlying sediments in the Taiwan region. The suggested upper-bound age for the breakup unconformity coincides with the age (∼ 30 Ma) of the oldest magnetic anomaly C11 found in the vicinity of the continent–ocean boundary (Taylor & Hayes, 1983; Briais *et al.*, 1993) (see Fig. 1).

Post-breakup strata

Figure 10 shows the isopach of the Oligocene–Miocene post-breakup strata. This sedimentary package accumulated between the initiation of the seafloor spreading of the South China Sea at ∼ 30 Ma and the onset of the arc–continent collision at ∼ 6.5 Ma (6.5 Ma is the age for the basal foreland unconformity, see later). The post-breakup sequence is thus floored by the breakup unconformity and topped by the basal foreland unconformity.

The Oligocene–Miocene post-breakup succession shows a sharp increase in thickness across the ENE-trending Yichu Fault in the south (Fig. 10). The Yichu Fault clearly separates the post-breakup sedimentary thickness into inner
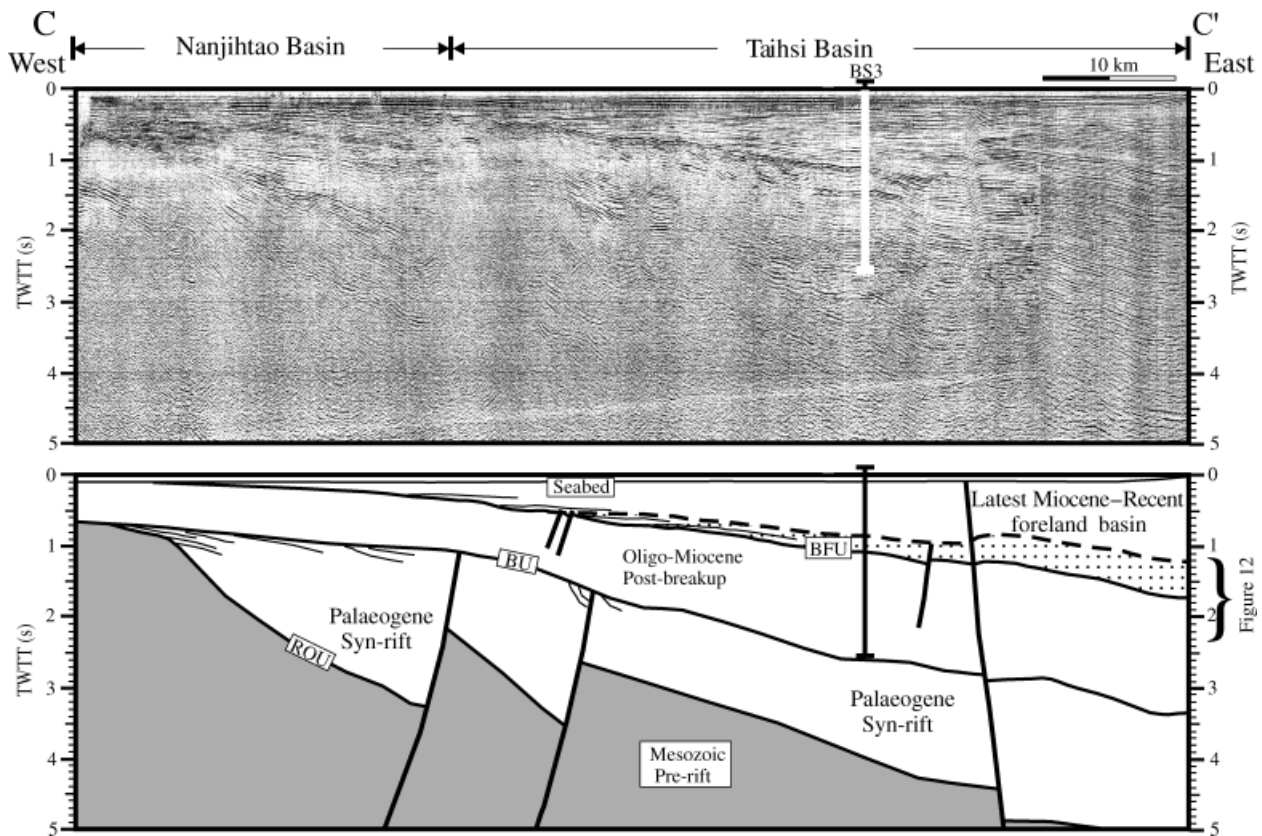
Fig. 7. Seismic section CC′ (see Fig. 2 for location) showing a notable onlapping feature associated with the basal foreland unconformity (BFU). Figure 12 shows the transitional stratigraphy from the rifted margin to the foreland basin along and in the vicinity of the eastern portion of this seismic section.

and outer regions. In the inner region, up to 3 km of fluvial to marine strata blanket the entire region, with sediments gradually thickening toward preceding rift centres and thinning toward basement highs. This is especially evident in the Taihsi Basin. The rather uniform thickness of the postbreakup strata and the lack of Oligocene–Miocene normal faulting in the inner region can also be seen from various seismic sections (see Figs 5–7, for example).

In contrast, in the outer region, marine sediments up to 6 km thick were ponded in the Tainan Basin (Fig. 8). The post-breakup sequence in the Tainan Basin appears, on the basis of seismic and borehole data, to be a thick, Miocene marine shale floored by a thin upper Oligocene transgressive sandstone unit, which rests unconformably upon the Lower Cretaceous. We interpreted that the thick post-breakup strata in the outer margin is a result of multiple stages of lithospheric extensions (see later).

Latest Miocene–Recent foreland basin (∼6.5–0 Ma)

The basal foreland unconformity separates an onlapping foreland basin sequence above from passive margin sequences below, and was first reported by Lin (2001) and Yu & Chou (2001) to mark the base of the Taiwan foreland sequence. The unconformity is best shown in the Taihsi

Basin and the Penghu Platform (Figs 6 and 7). In the Taihsi Basin, the basal foreland unconformity passes laterally into conformity toward the orogen where the basal foreland surface separates the Nanchuang Formation from the overlying Kueichulin Formation (Fig. 12). The age of this basal foreland surface is estimated, in this study, to be about 6.5 Ma and is in the upper part of zone NN11 according to (Fig. 12) (1) a recent K–Ar age determination (7.6–7.1 Ma) from a basalt layer ∼25 m beneath the boundary (Juang, 1996), (2) an age-diagnostic nannofossil, *Discoaster quinqueramus* first-occurrence/last-occurrence 8.6/5.6 Ma identified from a sidewall core sampled from the upper Nanchuang Formation, and (3) *D. quinqueramus* occurrence in the lower Kueichulin Formation.

The depth map of the basal foreland unconformity (Fig. 11) is obtained by correlating the basal foreland unconformity in the Taiwan region. The base of the foreland sequence (Fig. 11) generally forms a simple flexural downwarp, increasing its depth toward the orogen. The foreland flexure shows two segments distinct in terms of their geometry. These two segments are divided near Fault B in the east-central part of the Penghu Platform. The north segment of the foreland flexure lies on the Kuanyin Platform, Taihsi Basin and the northern part of the Penghu Platform, where a rift and thermal event occurred during ∼58–30 Ma, and exhibits minor normal faulting related to foreland flexure (Figs 6 and 7).
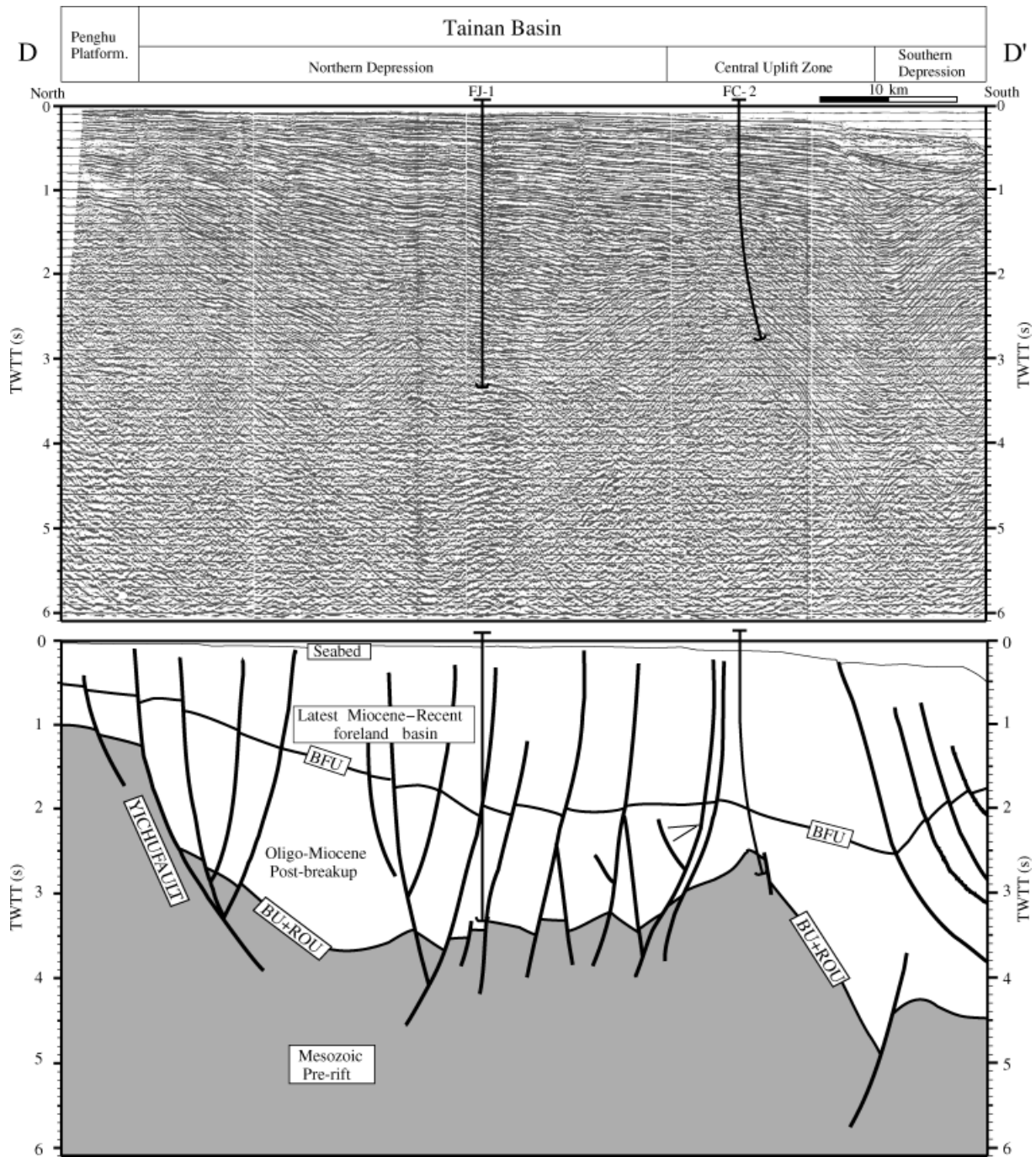
Fig. 8. Seismic profile DD′ (see Fig. 2 for location) across the Tainan Basin. The Tainan Basin is a fault-bounded, Oligocene–Miocene post-breakup basin superimposed by the late Cenozoic foreland sequence. The basin infills are block-faulted.

By contrast, the south segment of the foreland basin has developed mainly on top of the southern Penghu Platform and the Tainan Basin, where the lithosphere had experienced two more recent rift/thermal episodes from ∼30 to 21 Ma and from ∼12.5 to 6.5 Ma (see below). The south segment exhibits three fundamental differences from its northern counterpart: (1) the basal foreland surface is penetratively faulted and the normal faulting is clustered especially at the NE region along the Yichu Fault and bounded to its north by Fault B; (2) the strike of the fore-land flexure is concordant to the strike of the previous rift centre and is oriented at a high angle to the NS-trending Taiwan orogen; and (3) the curvature of flexure is high, as seen by the flexure at the thrust front, which is some 6 km deep as opposed to ∼3 km deep in the north segment.

The development of the foreland basin is strongly influenced by the thermo-mechanical structure of its underlying passive margin. This aspect is discussed fully in a separate paper (Lin & Watts, 2002).

Fig. 9. Sedimentary thickness (in km) of the Palaeogene pre-breakup sequence ($\sim$ 58–30 Ma). In the inner margin, syn-rift strata have accumulated in the Nanjihtao (NJB), Penghu (PHB) and Taihsi (TB) Basins. In the distal margin, few truncated rifts are present in the Penghu Platform and the northern extreme of the Tainan Basin. An Eocene sequence has been sampled from one of the truncated rifts at the IT1 well at the SW Penghu Platform. The equivalents are also exposed in the Backbone and Hsuehshan Range (see Fig. 2 for the geologic map). Seismic sections AA' to DD' are shown in Figs 5–8.
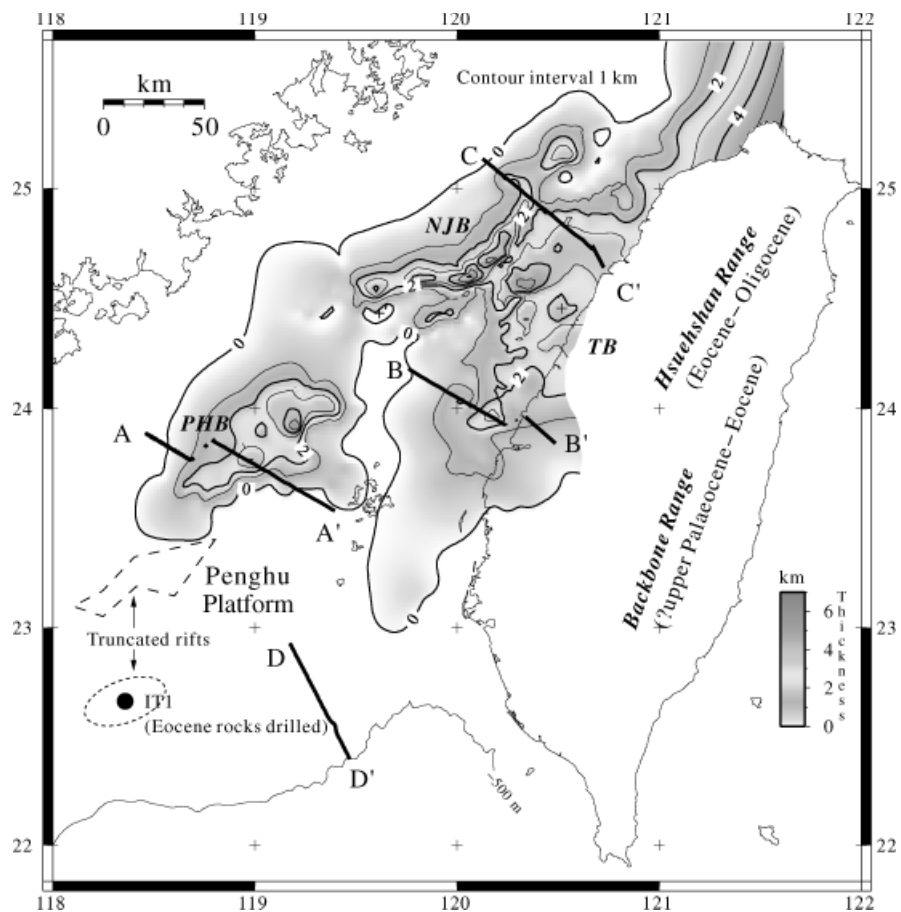
TECTONIC SUBSIDENCE AND UPLIFT HISTORY

Backstripping techniques (Watts & Ryan, 1976) were applied in order to determine the tectonic subsidence and uplift history of the South China Sea margin. This technique involves two main steps: decompaction and unloading. Decompaction seeks to restore the sediment thickness and density of individual layers throughout their burial history under the assumption of a porosity vs. depth curve that does not change through time. The porosity vs. depth relationship for individual basins and highs in the Taiwan region is constructed using the following steps: (1) the sonic velocity log (in the form of interval transit times) is converted to porosity and plotted against depth following the method of Raiga-Clemenceau *et al.* (1988) and Issler (1992), and (2) the average porosity–depth relation is determined by best fitting a mechanical compaction model curve (Audet, 1995, 1996) to the converted data. Figure 13 shows five representative theoretical porosity–depth curves from five basins/platforms and an example (the FJ1 well) of the conversion of sonic velocity to porosity. Figure 13 shows that the porosity–depth relationship can be reasonably well predicted by the mechanical compaction model of Audet (1995, 1996).

According to Audet (1995, 1996), two mechanical parameters are sufficient to describe a realistic porosity–depth function: the compression index (C_c, representing sedi-

ment strength) and the void ratio (e_{100}) at an effective stress of 100 kPa ($e_{100} = \varphi/(1 - \varphi)$, where φ is the porosity). The log-derived $C_c - e_{100}$ values can be checked by experimentally derived results. In doing so, the derived $C_c - e_{100}$ pairs were superimposed on plots of two empirically determined trends of Parasnis (1960), which tends to be more representative of calcareous sediments, and that of Burland (1990), which is more descriptive of clays (Fig. 13). Data points of $C_c - e_{100}$ pairs shown in Fig. 13 cluster along a well-defined linear trend and closely parallel the results for triaxial tests on clays of Burland (1990). The consistency of the log-derived and experimental results has further validated the use of the soil mechanics theory of Audet (1995, 1996) in predicting the porosity–depth relationship; also the compaction curve predicted in this way has provided an improved and physically based alternative in describing sediment compaction other than the classic, simple exponential porosity vs. depth relationships (e.g. Athy, 1930).

The predicted curves (Fig. 13) show an exponential reduction in porosity with increasing depth. The good agreement of the observed porosity and the model curves based on mechanical compaction also shows that mechanical compaction is the primary control on the reduction of porosity in the Taiwan region, reflecting the fact that the Taiwan Cenozoic sediments are predominantly siliciclastics in which the porosity reduction is due mainly to mechanical compaction (cf. Issler, 1992).
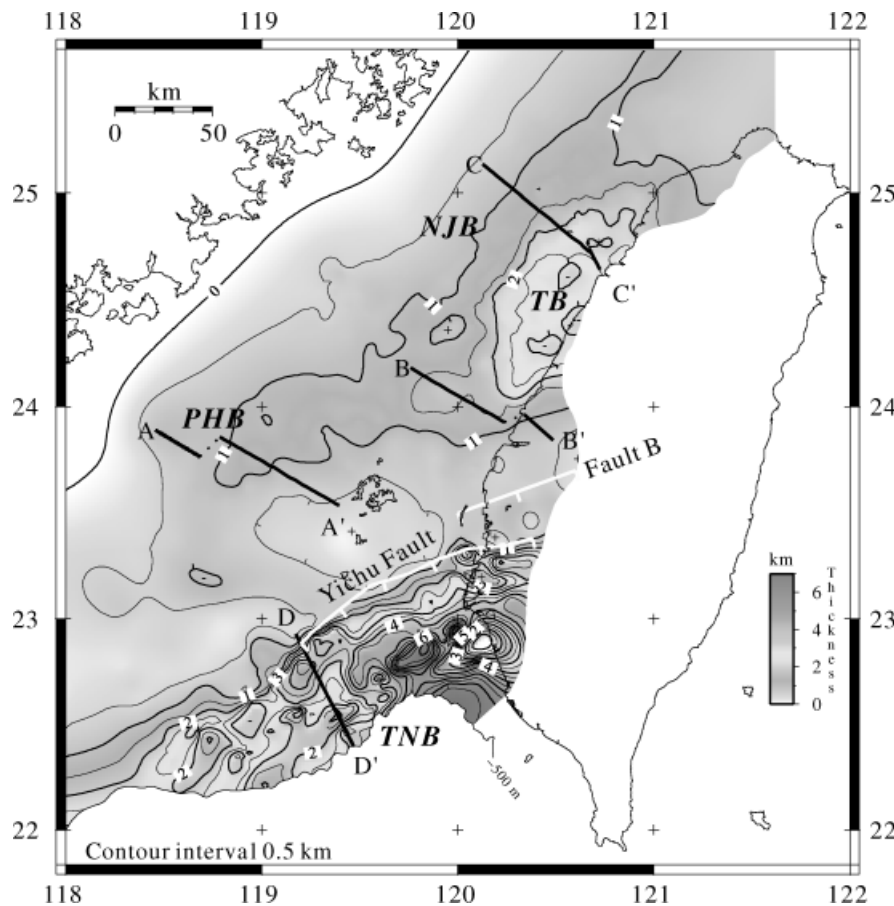
Fig. 10. Sediment isopach of the Oligocene–Miocene post-breakup sequence (∼30–6.5 Ma). Seismic section DD′ (Fig. 8) illustrates the structure of the Tainan Basin. Other seismic sections (AA′ to CC′) are shown in Figs 5–7, respectively. See Fig. 17 for post-breakup tectonic development.

Figure 14 shows the tectonic subsidence obtained by backstripping the sediments at a selection of wells aligned along the strike of the west Taiwan foreland basin and obliquely across the south China margin. The wells were backstripped according to their respective porosity–depth functions for individual tectonic regions shown in Fig. 13. The fully compacted basement was selected either at the top of the Mesozoic (basement) rocks or at the total well depth. The water depth at the time of deposition for the backstripped strata was also considered in calculating the tectonic subsidence. The range of palaeobathymetry estimates was shown as an error bar at each point on the tectonic subsidence curve. Because the entire Cenozoic sediments in the west Taiwan basins accumulated in a fluvial to shelfal setting (e.g. Ho, 1986), the range for the palaeobathymetry is therefore small. Finally, the resulting tectonic subsidence and uplift has been corrected for the effect of eustatic sea level change using the 'smooth' sea-level curve of Watts & Steckler (1979).

There are three main features of the subsidence patterns (Fig. 14): (1) initial subsidence (Palaeogene): there is a rapid initial subsidence during late Palaeocene to Eocene at wells that penetrated the fault-bound syn-rift deposits; (2) rapid post-breakup subsidence (mid-Oligocene to Miocene): following a period of uplift and erosion associated with the Oligocene breakup unconformity (see later), a second relatively rapid subsidence recommenced in the mid-Oligocene, which was succeeded by a generally

exponentially decaying subsidence during the Miocene; and (3) rapid foreland basin subsidence (latest Miocene–Recent): the generally slow subsidence during the Miocene is followed by a relatively rapid concave-down subsidence since at least the early Pliocene.

Initial subsidence: palaeogene syn-rift

Figure 15 compares five representative subsidence curves from five basins/highs with theoretical subsidence curves. The theoretical curves were calculated using the finite-rifting model of Cochran (1983) by assuming a lithospheric stretching factor, β, in the range 1.1–2.2. The initial rifting event is assumed to have occurred during the interval 58–30 Ma, prior to the opening of the South China Sea.

From the comparison (Fig. 15), the subsidence pattern at the deepest wells, BD1 and DW1, can be explained by a rifting model with initial rifting at 58 Ma and a rift duration of 28 Myr. The lower bound of β can be estimated as ∼1.45 at BD1 and ∼1.55 at DW1 (solid lines for the BD1 and DW1 curves) if the Oligocene unconformity is treated as a nondepositional hiatus. The model curves, however, cannot explain all the subsidence patterns of all the wells. Main departures of the observed subsidence patterns from the theoretical curves are during (1) the Oligocene–Miocene post-breakup stage and (2) the Pliocene–Pleistocene. The late Palaeocene–Eocene rapid initial subsidence is localised to the rift centres of the Penghu Basin (DW1)

Fig. 11. Depth structure map of the basal foreland unconformity. The dashed bold lines show the pre-existing crustal inhomogeneity in terms of the 2 km/3 km (north/south segment) isopach of Cenozoic sediments that accumulated prior to orogenic loading. Seismic sections AA′ to DD′ are shown in Figs 5–8, respectively. A stratigraphic cross-section for the lower part of the foreland sequence and its underlying upper post-breakup succession across an east–west array of wells in the vicinity of seismic section CC′ is shown in Fig. 12. The subsidence pattern for the foreland basin at the labelled well locations is shown in Fig. 14.
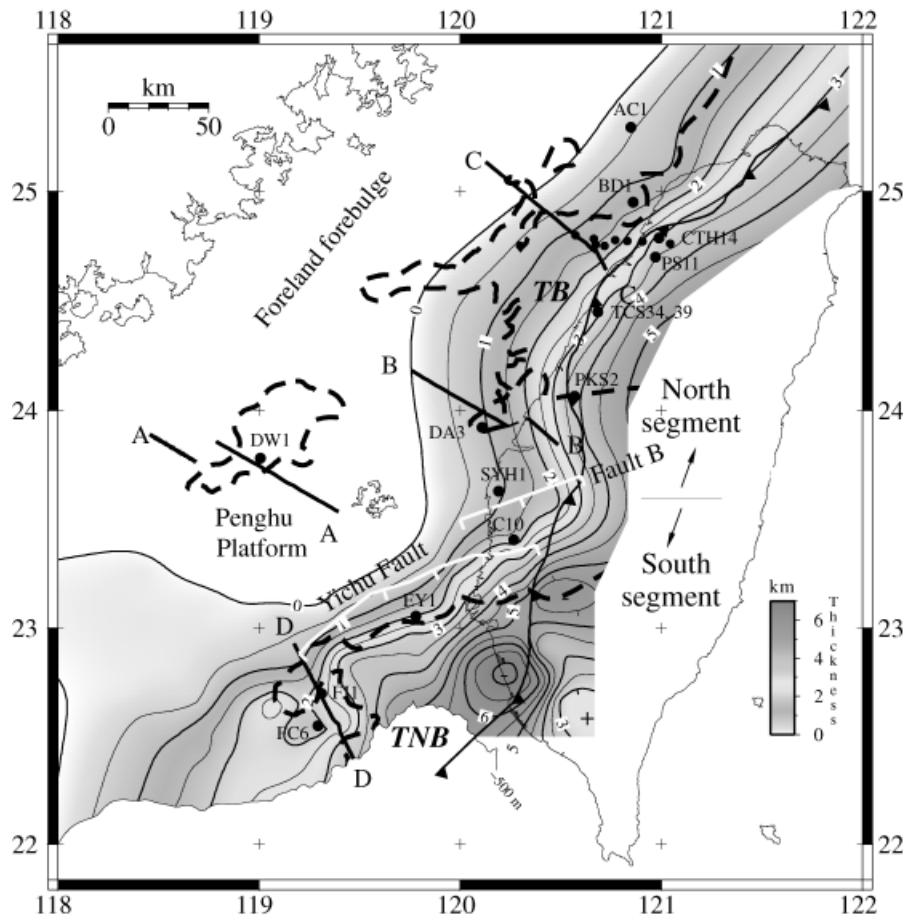
and the Taihsi Basin (BD1) as well as in the Nanjihtao Basin.

Anomalous post-breakup subsidence

The post-breakup subsidence ($\sim$30–6.5 Ma, Fig. 15) at the BD1 well appears anomalously rapid when compared with the predicted thermal subsidence, whereas the subsidence curve at the DW1 well closely resembles a post-breakup thermal subsidence curve.

Anomalously rapid post-breakup subsidence is also observed in most of the backstripped wells as shown in Fig. 14. In particular, the Oligocene–Miocene rapid subsidence in the outer part of the margin formed the fault-bounded Tainan Basin containing a block-faulted Oligocene–Miocene sequence. It is therefore reasonable to suppose that the rapid subsidence at the wells from the Tainan Basin (Fig. 14) may be due to some form of lithospheric extension that occurred following the commencement of seafloor spreading, i.e. post-breakup extension.

To test this possibility, a suite of observed subsidence curves at the outer margin are compared with theoretical ones in Fig. 16. The observed subsidence curve at FC6 shows a strong concave-up shape and a late Miocene hiatus, whereas other curves show a more linear, early subsidence pattern succeeded by a stepwise increase in subsidence rate in the late Miocene. The fact that the

subsidence pattern changed within a short distance (for example, 16 km is the distance between the FC6 and FJ1 wells) indicates that the tectonic process(es) that drove the post-breakup subsidence was locally focused rather than regional.

The theoretical curves were calculated by assuming one or two episodes of extension (Fig. 16 and Table 1). We acknowledge that the thermal model assuming two rifting events is not a complete model because the thermal effect generated by the first rift event is not considered in calculating the subsidence during the second rift episode. The results therefore are first-order approximations, especially for the second rift episode. The early (first) post-breakup extension is best seen at the FC6 well. At this well, a strong concave-up curve of 30–15 Ma duration can be predicted by a model curve, assuming that the lithosphere was thinned by a factor of 1.5 during 30–19 Ma immediately following the onset of seafloor spreading of the South China Sea. Nevertheless, the theoretical curve depicting thermal subsidence fails to fit the observed curve at the FC6 well, which shows a slight uplift during the middle Miocene followed by a hiatus in the late Miocene. The late Miocene rapid subsidence at other wells can be best explained by a renewed extensional event with a rift duration of 12.5–6 Ma. The spatially varied subsidence and uplift pattern during the late Miocene suggests that the former rift centre in the vicinity of the FC6 well was at the rift flank
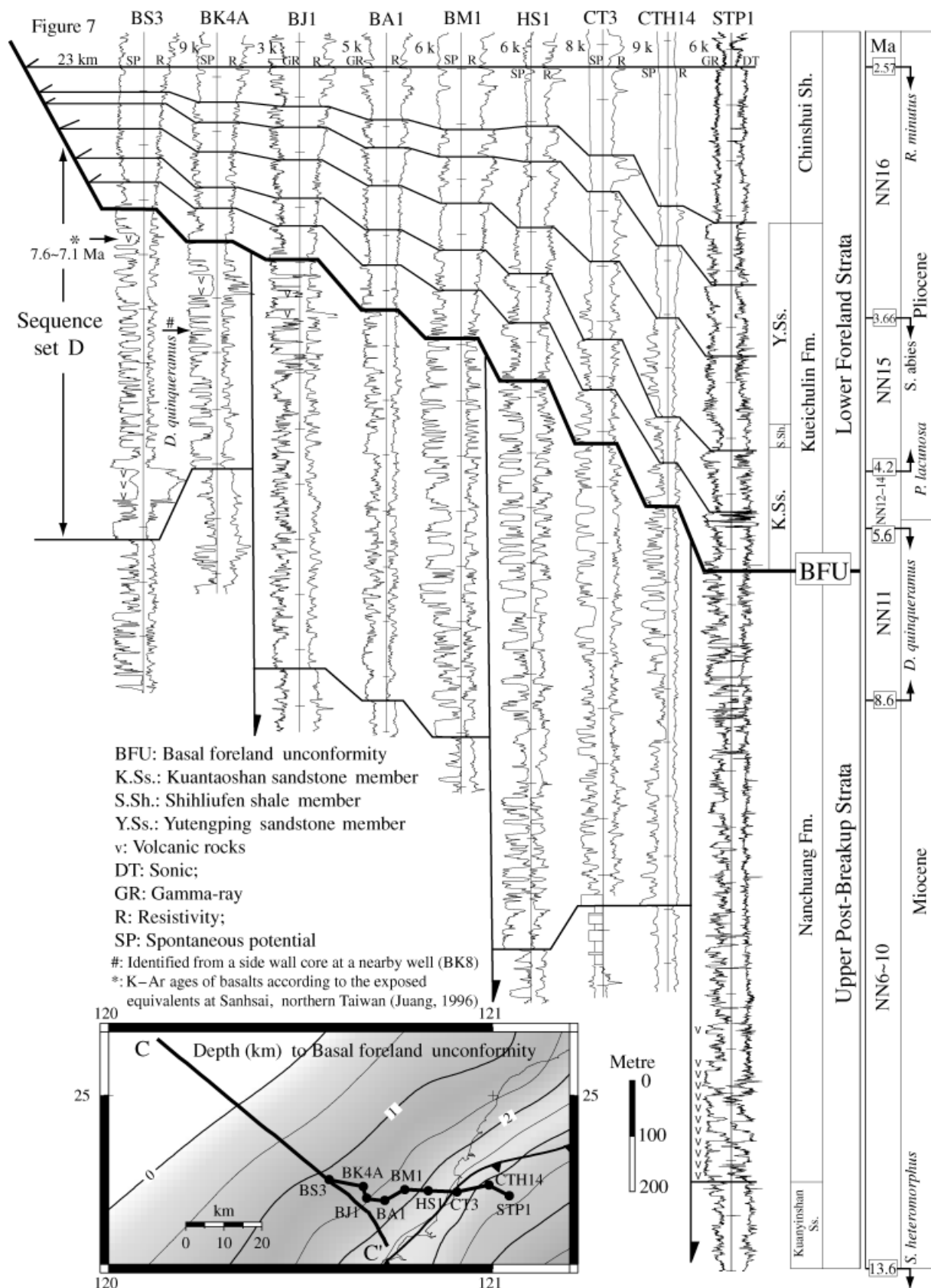
Fig. 12. Transitional sedimentation from a passive margin to a foreland basin setting on the north foreland segment. The basal foreland unconformity (BFU) separates the underlying upper Miocene post-breakup and fault-bounded fluvial to paralic strata from the eastward thickening, shallow-marine foreland strata that onlapped progressively onto the basal foreland unconformity in the west. See seismic line CC′ in Fig. 7 for the onlapping feature. Well locations are shown in the inset figure.
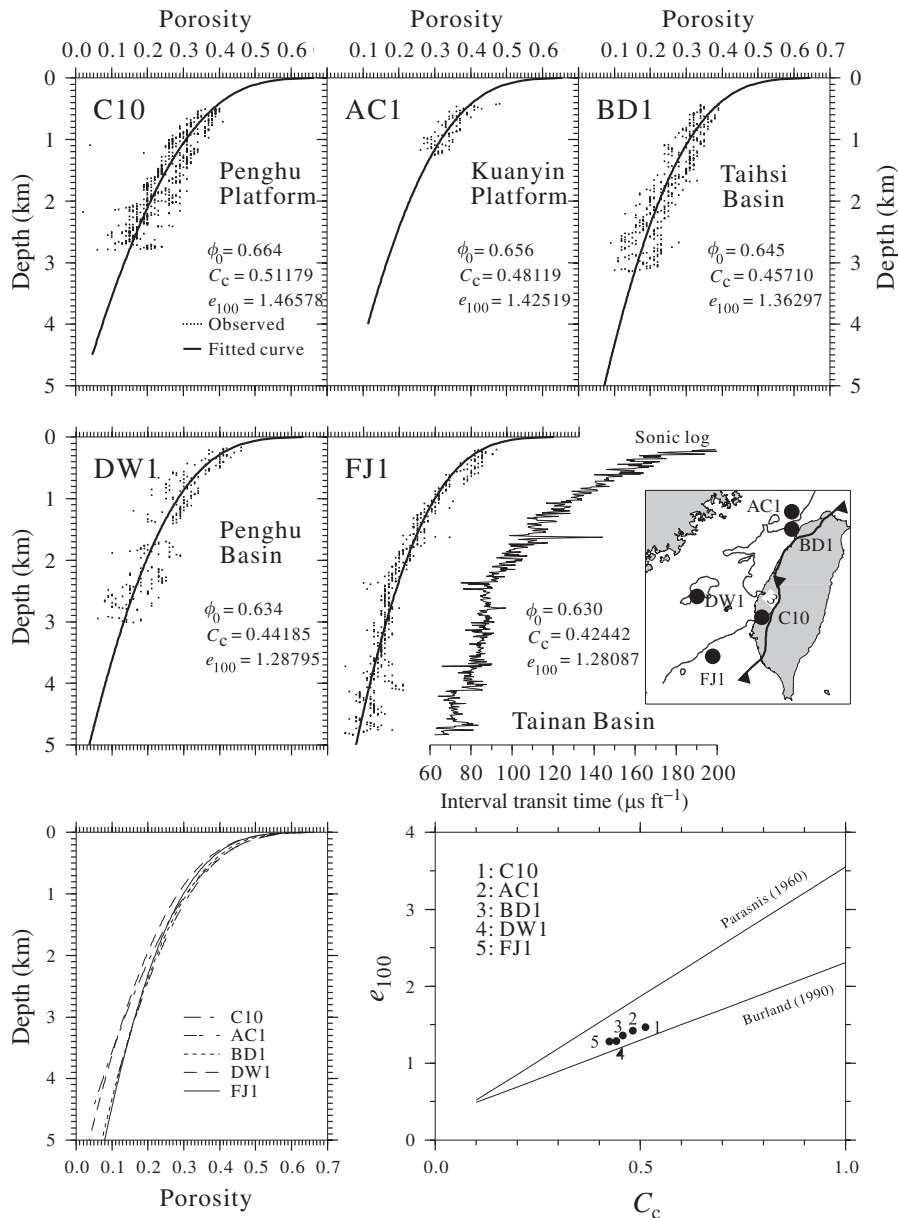
Fig. 13. Porosity–depth curves for the Cenozoic sediments from five tectonic regions. The initial porosity (φ_0), compression index (C_c) and void ratio (e_{100}) for individual wells together with one example (FJ1) for converting sonic interval transit time to porosity are also shown. The bottom-left figure shows a comparison for the five porosity–depth curves. The bottom-right figure shows that the derived five C_c–e_{100} pairs plot along a roughly linear trend. The inset figure shows the well locations and a 3-km isopach for the Cenozoic sediments depicting the depocentres and basement highs.

and experienced flank uplift during the second rift episode (see Fig. 17). Moreover, the first extension appears to be more widespread and greater in the amount of lithospheric stretching than that for the renewed late Miocene extension. Overall, the total stretching factor decreases toward the inner margin and β ranges from 1.58 to 1.22.

The anomalous early post-breakup subsidence in the outer margin can be largely explained by lithospheric stretching as has been shown above, and is evidenced by normal faulting; however, the contemporaneous rapid subsidence in the inner margin as seen in wells AC1, CTH14, PS11, TCS34+39 and PKS2 (Fig. 14) is associated

with a lack of major normal faulting. Instead, seismic reflection profiles and well data show that the early post-breakup strata in the inner margin have onlapped onto the neighbouring basement highs and have formed a classical 'steer's head' basin geometry (cf. Watts *et al.*, 1982), indicating a thermally controlled rather than fault-controlled subsidence following the development of the breakup unconformity.

In addition, there was a stage of rapid subsidence during the second rift episode ($\sim$ 12.5–6.5 Ma) as seen in the wells FJ1 and EY1 in the Northern Depression (ND) of the Tainan Basin (Fig. 16) and the wells PS11 in the Taihsi Basin
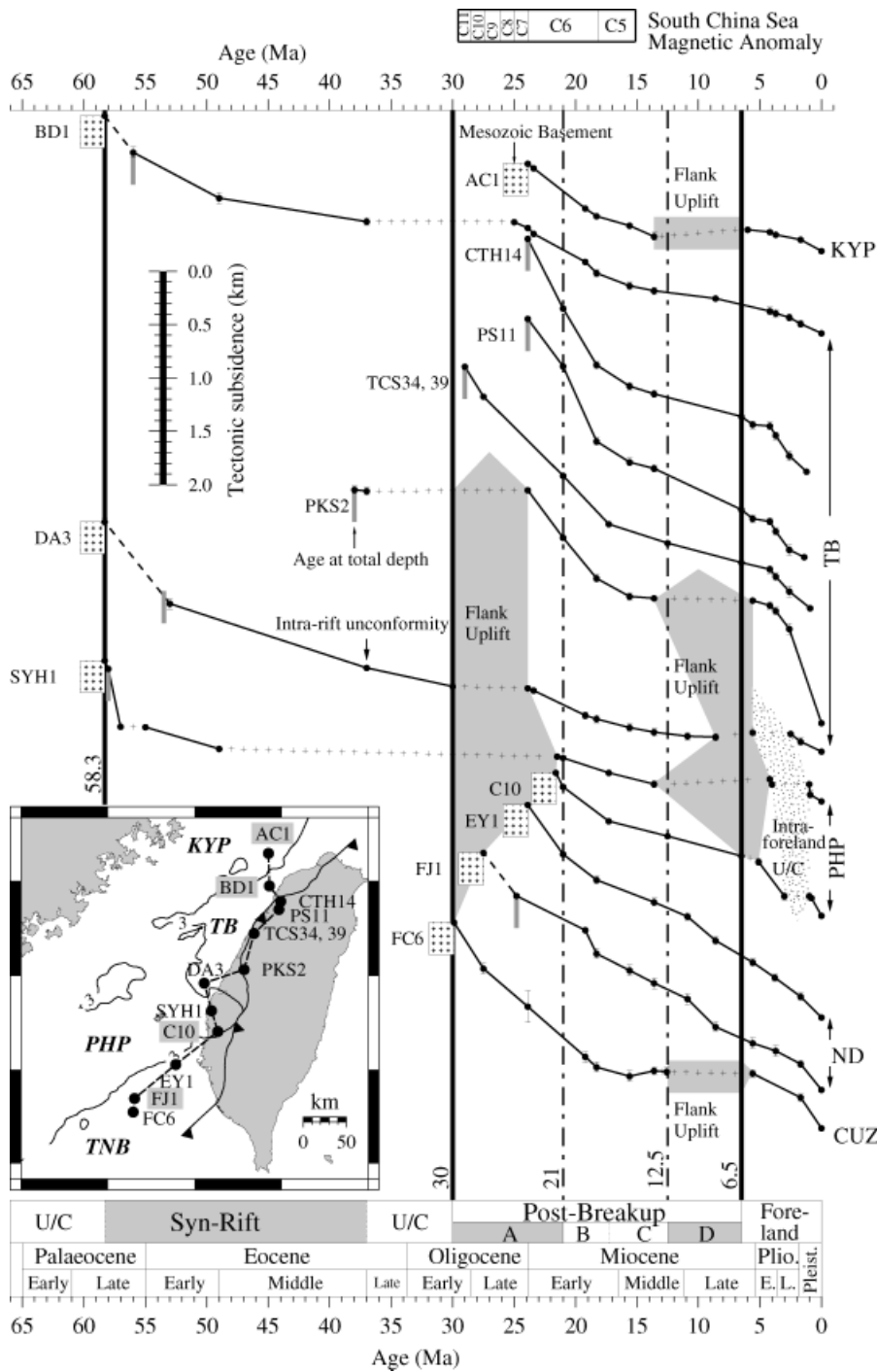
Fig. 14. Cenozoic tectonic subsidence pattern (lines) and the tectonic development of the west Taiwan basins (shown at the bottom of the figure, shaded box indicating rift episode). Also shown at the top of the figure are the seafloor magnetic anomalies of the South China Sea from Briais *et al.* (1993) according to the age model of Cande & Kent (1995). The vertical bar at dots (backstripping points) indicates the uncertainty in estimating the palaeobathymetry. The box with a plus pattern represents the Mesozoic basement and the vertical grey short line is the inferred age at the total well depth. Unconformity is treated as a nondepositional hiatus and is shown as crosses. The inset figure shows well locations and the names of the representative wells shown in Figs 13 and 15, respectively. U/C = unconformity.

(TB) (Fig. 14). The renewed extension in the Taihsi Basin is relatively mild and involved only normal faulting of several hundred metres as judged by the stratigraphic offset across faults (see Fig. 12, for example). In between, the rift flanks are characterised by an unconformity associated with non-deposition or uplift and erosion, such as the Central Uplift Zone of the Tainan Basin in the distal margin and the Penghu Platform bordering two rift centres.

The localised extension has segmented the west Taiwan basins into realms of rift centres and flanks as shown in the said subsidence pattern (Fig. 14). This subsidence pattern is further confirmed by sediment isopach maps shown in

Fig. 17. Stratigraphic data from ~200 boreholes have been used to establish the Oligocene–Miocene post-breakup stratigraphy (detailed in Lin, 2001). This succession is divided into 16 sequences, which can be grouped into four sequence sets (A, B, C and D). Sediment isopachs from these four sequence sets show that sequence sets B and C are of uniform thickness and drape the entire margin (Fig. 17b), whereas sequence sets A and D thicken into the fault-bounded troughs particularly in the Tainan Basin (Fig. 17a and c).

The post-breakup tectonic development can therefore be divided into three stages according to the above argu-
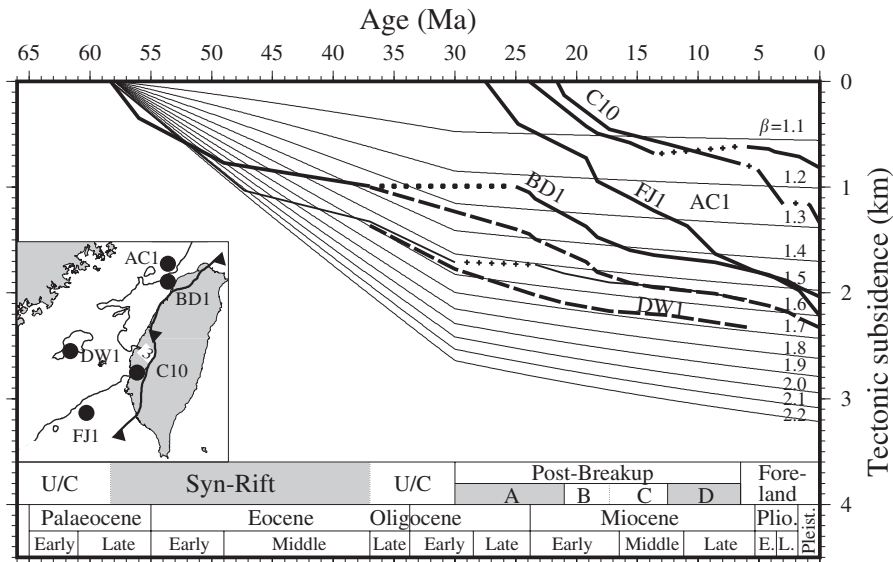
Fig. 15. Comparison of observed and theoretical subsidence curves for the five representative wells (Cl0: Penghu Platform; ACl: Kuanyin Platform; FJl: Tainan Basin; BDl: Taihsi Basin; DWl: Penghu Basin). Theoretical subsidence curves are shown for stretching factors, β, in the range 1.1–2.2. The dashed line for the subsidence curves of BDl and DWl are based on the 'restored' stratigraphy, taking into account the amount of erosion registered at the Oligocene breakup unconformity shown in Fig. 19.

ments (Fig. 17): (1) ~ 30–21 Ma, first post-breakup extension; (2) ~ 21–12.5 Ma, thermal subsidence; and (3) ~ 12.5–6.5 Ma, second post-breakup extension.

There is also a correlation in the timing of volcanism and lithospheric extension. The post-breakup volcanism in the Taiwan region has been grouped into two major eruptive phases, the Kungkuan Stage (23–20 Ma) and the Chiaopanshan Stage (13–7.1 Ma) (Ho, 1986; Chung *et al.*, 1994; Juang, 1996). Between these two Stages is a period of subdued basaltic eruption termed the Chienshih stage by Ho (1986). The two major basalt eruptive phases of the Kungkuan and Chiaopanshan Stages correspond approximately to the suggested two-stage post-breakup extension during the intervals ~ 30–21 and ~ 12.5–6.5 Ma, whereas the intervening thermal subsidence period from ~ 21 to 12.5 Ma correlates to the Chienshih Stage with minor basaltic eruptions.

Coeval with the late Miocene Chiaopanshan volcanism in the Taiwan margin was a phase of thermal metamorphism of greenschist facies (< 12 Ma, Lan *et al.*, 1990) that is observed in the Mesozoic complex in the Backbone Range. This thermal event has since been attributed to initial arc–continent collision in the then outer continental margin (e.g. Lan *et al.*, 1990; Teng, 1990; Lo & Yui, 1996), even though the sedimentary records appear to indicate that the arc–continent collision was initiated at a later time at ~ 5 Ma (cf. Teng, 1990) or at ~ 6.5 Ma as suggested in this study. An apparent alternative cause for this thermal event prior to initial orogenic loading is the ~ 12.5–6.5 Ma extension that occurred primarily in the outer margin.

Foreland basin subsidence

The rapid subsidence since the early Pliocene departs from the backstripped curves typical of extensional basins, as it is
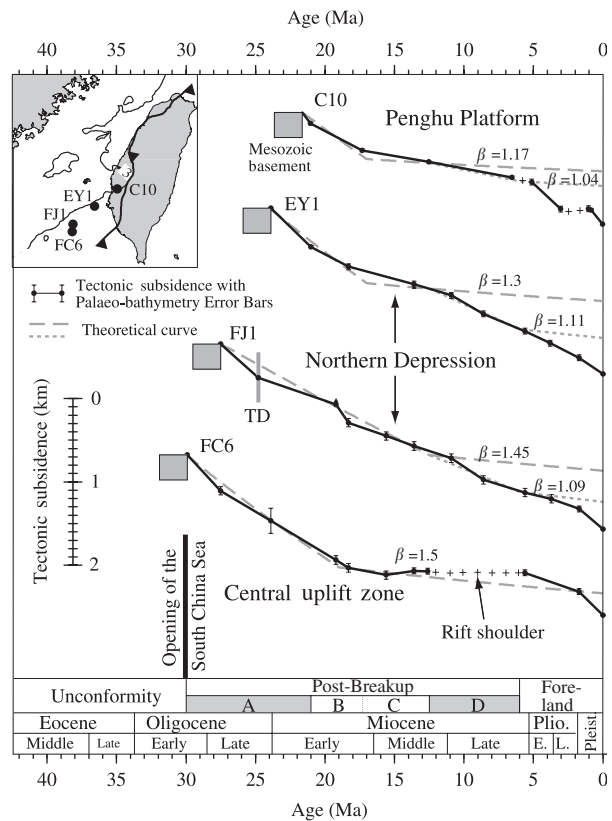

Fig. 16. Observed and calculated subsidence curves at the outer margin wells (Cl0 for the Penghu Platform; EYl, FJl and FC6 for the Tainan Basin).

concave down. A subsidence curve that is concave down is characteristic of (although not exclusive to) foreland or compressional basins (e.g. Watts, 1992; Haddad & Watts, 1999).

**Table 1.** Durations and stretching factors, β, of two post-break-up extensions in the outer margin.

Well	First extension	Second extension	Total stretching factor
C10	21.6–17 Ma ($\beta = 1.17$)	12.5–6 Ma ($\beta = 1.04$)	1.22
EY1	24–17 Ma ($\beta = 1.3$)	12.5–6 Ma ($\beta = 1.11$)	1.44
FJ1	27.5–12.5 Ma ($\beta = 1.45$)	12.5–6 Ma ($\beta = 1.09$)	1.58
FC6	30–19 Ma ($\beta = 1.5$)	None (flank uplift)	1.50

The concave-down subsidence pattern that begins in the early Pliocene can be interpreted as the result of loading in the Taiwan orogen caused by the collision of the rifted margin and the Luzon arc (e.g. Teng, 1990). The loading event has formed a foreland basin to the west of the Taiwan orogen since about 6.5 Ma, as suggested from the age of the basal foreland unconformity. Rapid foreland subsidence did not start, however, until about 4 Ma. Foreland subsidence was therefore initially slow, but accelerated through time because of the progressive advancement of the orogenic loads onto the passive margin. The foreland subsidence has occurred, however, at places within about 100 km from the thrust front. In contrast, the Penghu Basin (DW1) has been at the foreland forebulge, where the upper Miocene sediments have been exposed on the seabed (Fig. 5), and hence no synchronous Pliocene–Recent subsidence is seen at the DW1 well. The porosity–depth relationship at the DW1 well (Fig. 13) shows a normal compaction curve, suggesting that the upper Miocene sequence has remained near the present position ever since its deposition.

RIFT–DRIFT TRANSITION AND THE DEVELOPMENT OF BREAKUP UNCONFORMITY

The establishment of normal compaction curves in the Taiwan region (Fig. 13) allows the amount of erosion asso-
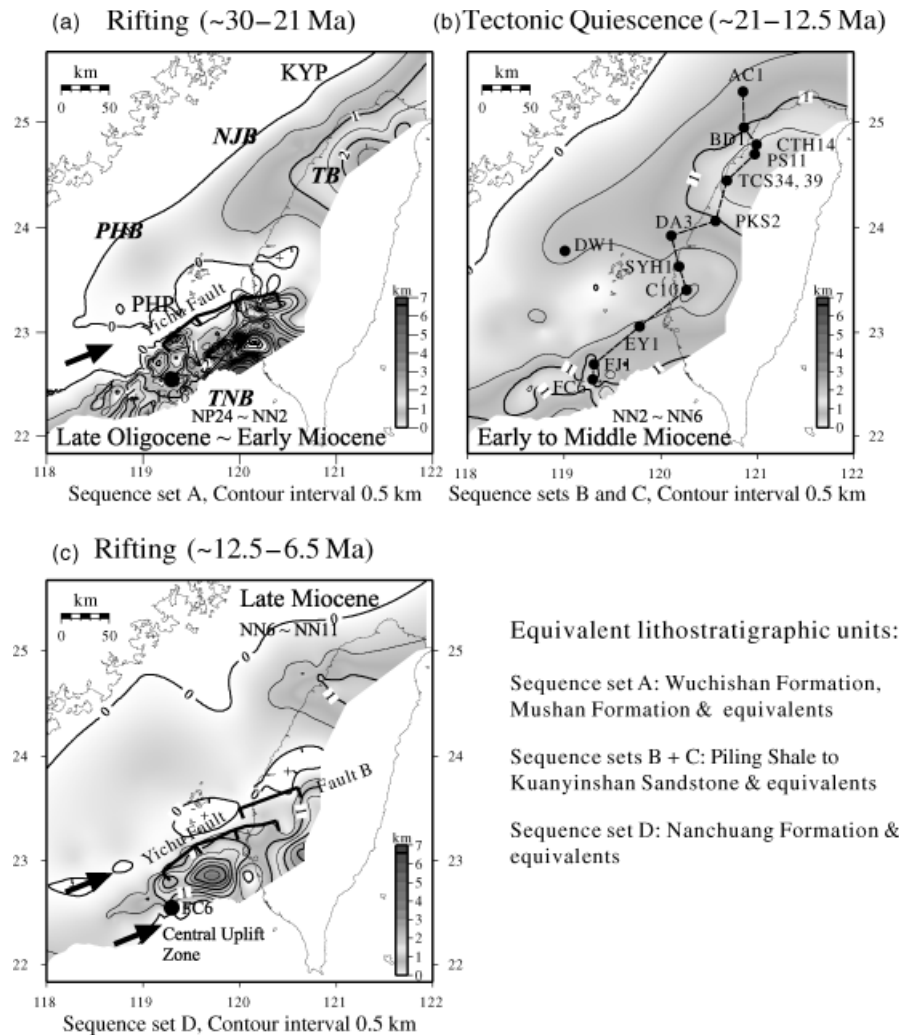
Fig. 17. Post-breakup tectonic development in the Taiwan region (~ 30–6.5 Ma). Arrows indicate rift flanks. See Fig. 10 for the total thickness of the post-breakup sequence and Fig. 14 for the subsidence pattern at wells shown in (b).

ciated with the development of major unconformities to be quantified. The amount of uplift and erosion can be estimated by comparing observed and normal compaction curves, provided the following assumptions hold: (1) Porosity reduction with increasing burial depth is caused solely by mechanical compaction. Other factors, such as diagenesis and dissolution, do not affect porosity variation with depth. (2) Depth-controlled compaction is irreversible. Hence the porosity is not reversed by subsequent uplift. (3) All stratigraphic units follow a normal porosity–depth curve. The above assumptions are largely justified in the study area as the Taiwan Cenozoic sediments comprise mainly siliciclastics with low contents of total organic carbon.

There is a sharp offset in the porosity–depth curve across the breakup unconformity when shallowly buried (e.g. < 1000 m, Fig. 18). Porosity is much lower below the unconformity than above it, suggesting that the breakup unconformity is associated with uplift and erosion. Only wells that penetrated the breakup unconformity, which separates Palaeogene syn-rift sediments from the overlying post-breakup strata (diamonds in Fig. 19), are used in estimating the amount of erosion. The anomalously low porosity zone of the Palaeogene sediments is only observed in the Penghu Platform and the southern Taihsi Basin (solid diamonds in Fig. 19), where the depth of post-Oligocene re-burial is shallower than the maximum burial depth that the Palaeogene sediments experienced.

The amount of material removed is estimated by the following steps (Fig. 18): (1) Overlay the observed porosity data and normal compaction curves. Two end members of compaction curves, i.e. DW1 and FJ1 curves, are plotted for reference. The DW1 curve, which lacks the foreland infill component, is taken as the normal compaction curve that best describes the state of sediment compaction prior to continental breakup. (2) Move the anomalously low porosity zone beneath the breakup unconformity vertically down along the depth axis until a good fit of the observed data and DW1 reference curve in terms of root mean square (rms) residual is achieved. (3) The amount of material that has been removed by erosion can be taken as the depth difference between the present-day sea level and the restored upper surface of the anomalous porosity zone.

At the inner margin wells, the deeper post-Oligocene re-burial (e.g. > 1300 m) has resulted in an apparent 'normal' porosity–depth curve, which shows no abrupt change in porosity across the breakup unconformity. In this case, the amount of material removed is considered to be less than the present-day depth of the breakup unconformity. The depths of the breakup unconformity at selected wells showing 'normal' compaction trends and shallow post-Oligocene re-burial (e.g. at CT1, DA3 and DW1 wells, unfilled diamonds in Fig. 19) are therefore used as an upper bound for the amount of material that has been removed by Oligocene uplift and erosion. Finally, the Oligocene continuous sedimentation, i.e. no uplift and erosion, in the Hsuehshan Range (Teng *et al.*, 1991) is restored to its origi-
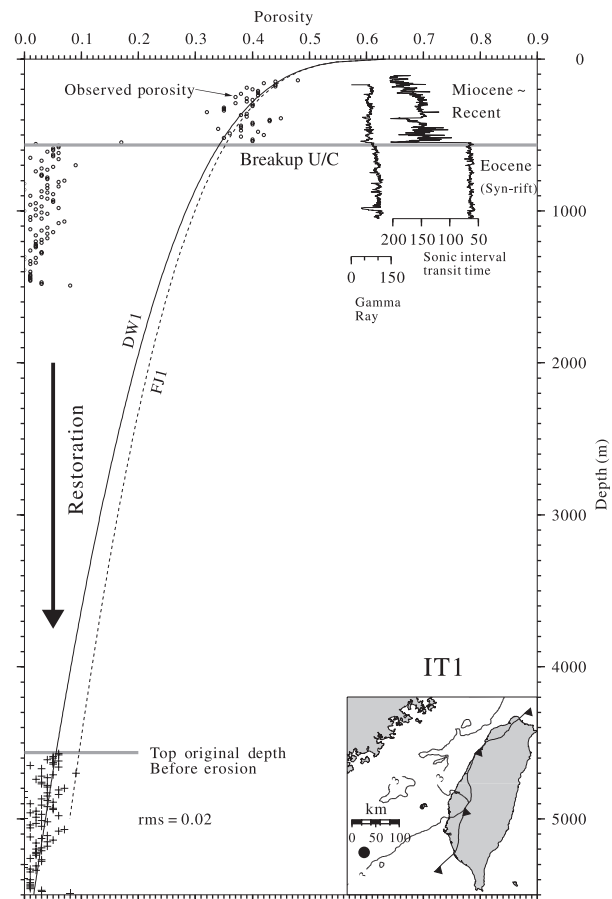

Fig. 18. Plots of observed porosity (unfilled circles), log curves of gamma ray and sonic interval transit time of the IT1 well together with reference porosity–depth curves of DW1 and FJ1. The root mean square (rms) residual between the DW1 reference curve and 'restored' porosity is 0.02 (or 2%).

nal position according to a retrodeformed (balanced) cross-section suggested by Suppe (1980) (solid triangle, HR, in Fig. 19).

Figure 19 shows in map form the amount of material removed by the uplift and erosion associated with the development of the Oligocene breakup unconformity. The erosion is of long wavelength and large amplitude, with a cumulative amplitude of up to 4500 m centred at the IT1 well. It also trends parallel to the strike of the South China continental margin, with the largest erosion running along the southern Penghu Platform, where the average amount of cumulative erosion is in the order of some 2500–3000 m. Fuh (2000) also concluded that an Oligocene erosional event affected the Taiwan region with up to 3500 m of erosion on the Penghu Platform using a sonic velocity vs. depth relationship, but assuming a linear rather than exponential trend for compaction curves.

There are two points worth noting: (1) the scale of the uplift and erosion, especially the amplitude, is a cumulative effect spanning ~ 37–30 Ma and should not be considered the result of an instantaneous event; and (2) there may be a contribution to the uplift/erosion from local
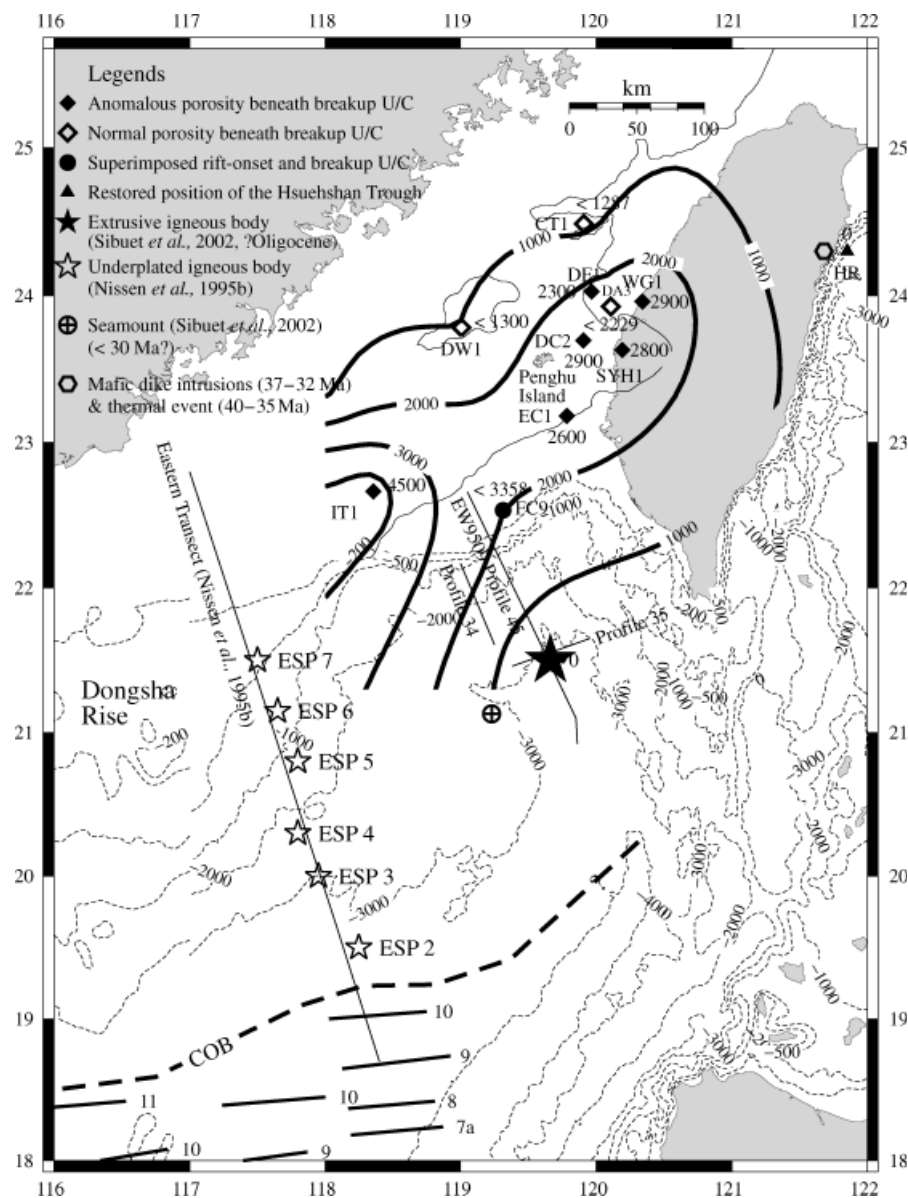
Fig. 19. Contours (thick line, in metres) of the amount of erosion associated with the development of the Oligocene breakup unconformity during the rift–drift transition (~ 37–30 Ma). More or less coeval events with the development of the Oligocene breakup unconformity were magmatic underplating (unfilled stars) beneath the Dongsha Rise (cf. Nissen *et al.*, 1995b), extrusive (filled star) off SW Taiwan (cf. Sibuet *et al.*, 2002), mafic dike intrusion and a possible thermal metamorphism in the Backbone Range (Jahn *et al.*, 1986; Lan *et al.*, 1990). These known coeval events all occurred in the outer margin and near the continent–ocean boundary (COB). The seafloor magnetic anomalies (C11n to C7a) and continent–ocean boundary are from Briais *et al.* (1993).

fault-block rotation and uplift that predates the breakup unconformity. For example, Yielding (1990) suggested footwall erosion of the tilted fault blocks in the northern North Sea to be between 100 m and 1.4 km.

A contributing, rather than an alternative, cause of the large amount of erosion associated with the breakup unconformity is a eustatic sea-level fall in the mid-Oligocene. The sea-level fall has been variously estimated as 400 m (Vail *et al.*, 1977), 130 m (Haq *et al.*, 1987) and 30–50 m (Miller *et al.*, 1985), and occurred at ~ 30 Ma (Miller *et al.*, 1998). Although the estimated magnitude varies, the sea-level fall will certainly enhance the amount of erosion during crustal uplift. However, it cannot explain the relative large amount of erosion (up to 4500 m) alongstrike of the South China margin.

One problem with backstripping is restoring the stratigraphy in the presence of major unconformities. The estimated erosion associated with the Oligocene breakup unconformity was then added back to restore the stratigraphy in estimating the stretching factor, β, at deep wells (dashed curves of DW1 and BD1 in Fig. 15). The 'restored' tectonic subsidence curves at the above two wells show that the stretching factor is in the range ~ 1.55–1.7.

DISCUSSION

We have shown that the west Taiwan basins have evolved from a Palaeogene rift to a latest Miocene–Recent foreland basin, and that this evolution is related to the opening of the South China Sea and its closure by orogeny in the Taiwan region. The development of the South China margin in the Taiwan region, however, appears to be anomalous when compared with other Atlantic-type passive margins (e.g. East USA margin, Steckler & Watts, 1978). The 'normal' passive margin generally lacks evidence of further extension following the inception of the seafloor spreading and undergoes regional thermal subsidence (e.g. Steckler & Watts, 1978). Also, a margin-scale uplift during rift–drift transition is rarely documented in the literature for a 'normal' passive margin, although the presence of an extensive breakup unconformity in these margins is a norm (e.g. Falvey, 1974; Hubbard *et al.*, 1985; Hubbard, 1988; Grow *et al.*, 1988). In this sense, the anomalous features in the north South China Sea margin in the Taiwan region include: (1) a margin-scale uplift and erosional event is associated with the formation of the Oligocene breakup unconformity (Fig. 20b); and (2) two stages of rapid subsidence associated with rifting occurred following the continental breakup (Fig. 20c and e). In this section, a possible mechanism is discussed to explain the tectonic development of the Taiwan rifted margin prior to orogenic loading.

The Oligocene uplift and erosion event ($\sim$37–30 Ma, Fig. 20b) post-dates the late Palaeocene–Eocene rifting ($\sim$58–37 Ma, Fig. 20a) by at least 20 Myr. The Oligocene uplift also occurred several Myr prior to the onset of seafloor spreading, $\sim$30 Ma, in the south along the continent–ocean boundary. During the rift–drift transition and final continental breakup, all the preceding loci of crustal thinning in the Taiwan region were abandoned and elevated as flank mountains with respect to the future site of continental rupture. The flank mountains, however, were a transient feature. They were lowered quickly below sea level by the rapid subsidence ($\sim$30–18 Ma) that followed the initiation of spreading in the South China Sea (Fig. 20c).

In addition, during the rift–drift transition (Fig. 20b), there was thermal metamorphism accompanied by mafic dike intrusions in the outer margin and vigorous magmatism producing both extrusive and underplated igneous bodies near the continent–ocean boundary.

Recent deep seismic surveys (EW9509) off SW Taiwan have revealed extrusive bodies (up to 3.5 s in two-way travel time in 'thickness' reported in Sibuet *et al.* (2002)) in the continental slope (Fig. 19). High-velocity material beneath the Dongsha Rise off SW Taiwan (Nissen *et al.*, 1995a, b) (Fig. 19) is interpreted, in this study, as magmatic bodies that underplated the stretched continental crust (see later).

Lin (2001) correlated the seismic reflectors of the EW9509 seismic sections reported in Sibuet *et al.* (2002) to the geology beneath the adjacent shelf and found that the top of the extrusive body corresponds approximately to the Oligocene breakup unconformity. For this reason, the extrusive igneous body is most likely to be associated with the development of the Oligocene breakup unconformity, and is interpreted to be emplaced during the rift–drift transition or shortly following the opening of the South China Sea.

Seismic refraction data across the Dongsha Rise off SW Taiwan (Nissen *et al.*, 1995a, b) (Fig. 19) suggest the existence of a high-velocity lower crust there (7.0–7.5 km s^{-1}). The thickness of this high-velocity layer varies from a minimum of 2.8 km at ESP 2 to a maximum of between 12.2 and 17.2 km at ESP 7. Nissen *et al.* (1995b) interpreted the high-velocity material in the vicinity of ESP 2 as an underplated igneous body during rifting because of its association with a small packet of fan-shaped seaward-dipping reflectors at the base of the crust. Nissen *et al.* (1995b) considered, however, the other high-velocity layer to be a result of pre-existing crustal material or of a composite of pre-rift lower crustal material and intrusions of mantle instead of invoking magmatic underplating. Nissen *et al.* (1995b) rejected magmatic underplating as the sole cause for this body because of its anomalously large thickness (up to 13 km) and the apparent lack of accompanied extrusive volcanism. It is worth noting that the large extrusive body off SW Taiwan, reported in Sibuet *et al.* (2002), was previously unknown to Nissen *et al.* (1995b).

Consider the following: (1) As a result of melt enhancement, thick underplated layers, with thickness up to 15 km, are present beneath some margins, e.g. Hatton Bank and Rockall Plateau (White *et al.*, 1987), and these margins commonly exhibit significant amounts of extrusive volcanism. (2) The extrusive volcanism at the EW9509 line off SW Taiwan, which occurred adjacent to the high-velocity lower crust beneath the Dongsha Rise, may indicate that the high-velocity lower crust material and the extrusive body are related features and have been emplaced more or less during the same period of time. (3) The spatial distribution of the high-velocity lower crustal bodies coincides with a band of positive magnetic anomalies ($>$100 nT) over the Dongsha Rise (e.g. Hsu *et al.*, 1998). This band of positive magnetic anomalies extends northeastwards along the southern flank of the Penghu Platform and the northern Tainan Basin and reaches, at least, into south-central Taiwan. Close to Taiwan, Lee *et al.* (1993a) argued that magmatic underplating may have taken place in the Cenozoic based on studies on xenoliths that are contained in the Miocene Penghu basalts in the Taiwan Strait. This correlation indicates that the ENE-trending positive magnetic anomalies may be related to the presence of magmatic material in the crustal level. (4) Ludmann & Wong (1999) suggested that two stages of crustal uplifting occurred in the Dongsha Rise at the time of the Miocene/Pliocene boundary and post-Pliocene, respectively, based on an interpretation of a reflection seismic data set. They also interpreted these two uplift events to be associated with magma intrusion into the upper crust.

The above points indicate that the high-velocity lower crust beneath the Dongsha Rise is most likely to consist of magmatic rocks and is neither pre-existing crustal material nor a composite of pre-rift lower crustal material and
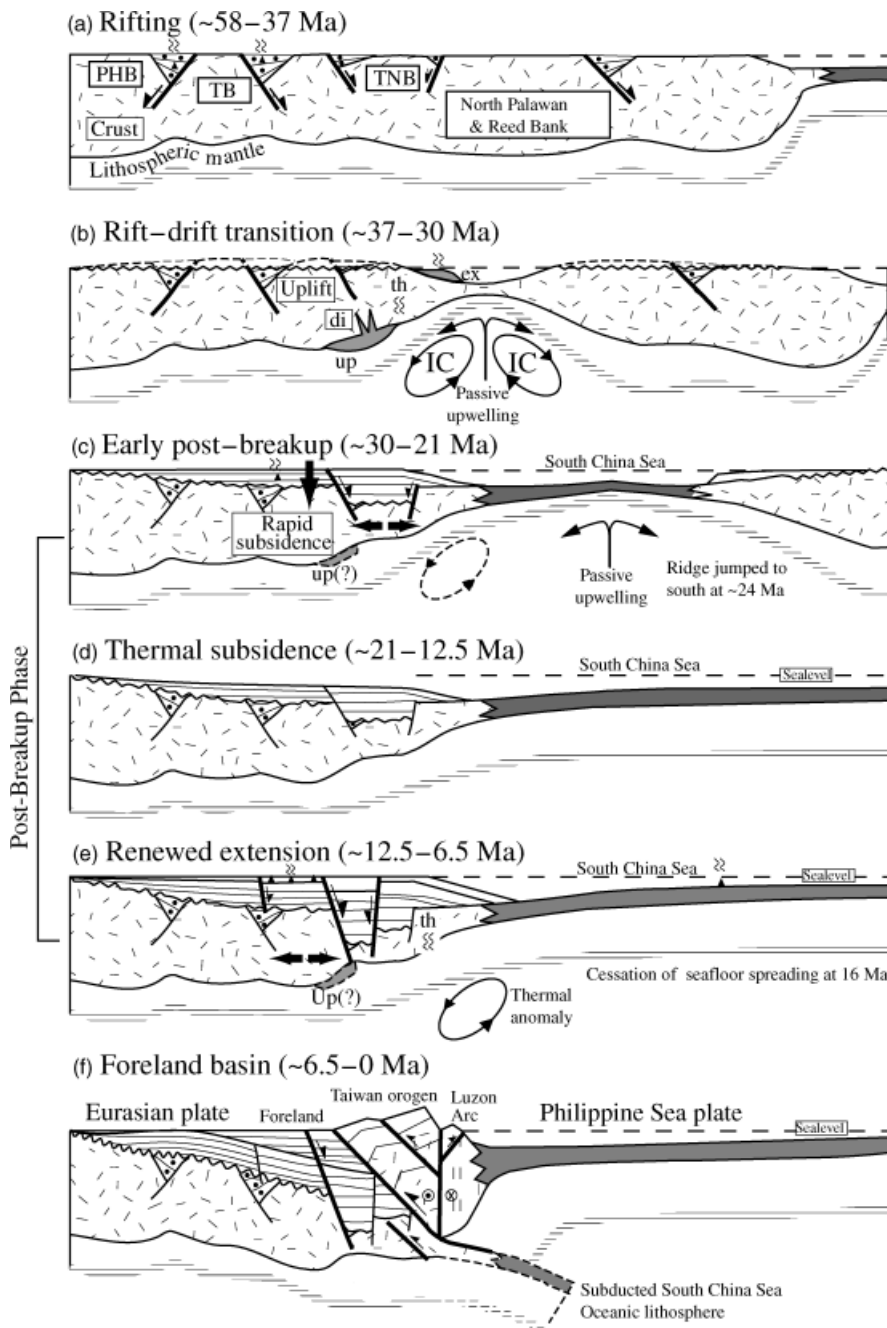
Fig. 20. Tectonic development of the northern South China Sea margin in the Taiwan region. See text for further discussion. di = dike intrusions, ex = extrusive rocks, IC = induced small-scale mantle convection, th = thermal metamorphism, up = underplated igneous bodies, PHB = Penghu Basin, TNB = Tainan Basin, TB = Taihsi Basin.

intrusions of mantle as perceived by Nissen et al. (1995b). The anomalously large thickness of these high-velocity bodies may be attributed to the following two causes or a combination of these two: (1) an enhanced mantle melting by introducing 'extra' heat during the rift–drift transition, which promotes mantle melting and produces an anomalously thick underplated igneous body; and (2) repeated magmatic underplating, possibly during the rift–drift transition ($\sim$37–30 Ma), early post-breakup extension ($\sim$30–21 Ma) and late Miocene post-breakup extension ($\sim$12.5–6.5 Ma) according to the tectonic development of the Taiwan region suggested in this study.

A phase of mafic dike intrusion in the Mesozoic basement complex in the Taiwan Backbone Range during $\sim$37–32 Ma (Jahn et al., 1986; Juang & Bellon, 1986) and a possible thermal (metamorphic) event about 40–35 Ma (Jahn et al., 1986; Lan et al., 1990) have been reported (Fig. 19). Jahn et al. (1986) related the $\sim$40–35 Ma thermal event to the opening of the South China Sea. The sudden increase in the temperature of this thermal event did not occur in the main phase of extension in the Taiwan margin during $\sim$58–37 Ma. It occurred instead during the final stage of continental rifting and prior to the onset of seafloor spreading of the South China Sea at $\sim$30 Ma.

All the above features (margin-scale uplift, vigorous magmatism and thermal metamorphism during the rift–drift transition as well as rapid early post-breakup subsidence) may be linked to an addition of heat and its

subsequent decay when final continental breakup became concentrated at (or jumped to) the present continent–ocean boundary. A heating event would have promoted transient (dynamic and/or isostatic) crustal uplift followed by rapid subsidence as heated lithosphere cooled; it can also explain the thermal event in the outer margin and vigorous magmatism that occurred adjacent to the continent–ocean boundary during breakup.

The margin-scale uplift in the Taiwan region may also be caused by magmatic underplating. This process is, however, considered as a subordinate mechanism because underplating tends to produce crustal uplift of a persistent rather than transient nature (cf. White & Mckenzie, 1989) and so does not explain the rapid subsidence following underplating. However, underplating may be an important mechanism in the Dongsha Rise (Fig. 19), as the Dongsha Rise has remained a positive feature since at least the Oligocene (e.g. Zhou *et al.*, 1995).

The introduction of extra lithospheric heat during the rift–drift transition may be an intrinsic part of the rifting process associated with the onset of seafloor spreading. Alternatively, the injection of heat may be due to a mantle plume impinging on the base of the lithosphere. However, there is little or no evidence of the existence of a mantle plume in and around the South China Sea (Tu *et al.*, 1992).

It has been shown that secondary convection beneath continental rifts may be generated if a strong lateral thermal gradient has been established as a consequence of rifting (e.g. Keen, 1985; Buck, 1986; Mutter *et al.*, 1988; Boutilier & Keen, 1999). Although the dynamics of such convection are poorly understood, its effects have been proposed to explain (1) margin-scale uplift bordering a continental rift zone, such as the margins bordering the Gulf of Suez (Buck, 1986; Steckler *et al.*, 1998); (2) the generation of excess magmatism and thick oceanic crust during the initial oceanic spreading phase, i.e. the generation of a volcanic continental margin (Mutter *et al.*, 1988; Zehnder *et al.*, 1990; Holbrook & Kelemen, 1993; Kelemen & Holbrook, 1995; Keen & Potter, 1995); and (3) an anomalously thick oceanic crust in young ocean basins (Martinez *et al.*, 1999).

As noted earlier, Palaeogene rifting occurred simultaneously in a > 200-km wide rift zone in the Taiwan region (Fig. 20a). Also, Zhou *et al.* (1995) have reported that Palaeogene rift structures exist in the conjugate margin to the south in the continental terranes of the Reed Bank and the northern Palawan block (Figs 1 and 20a). A wide rift is unlikely to be associated with rift-induced convection because the lateral thermal gradient and the topography of the asthenosphere/lithosphere boundary tend to be subdued (Mutter *et al.*, 1988). During the final stage of continental breakup, however, the intensive rifting became concentrated at (or jumped to) the present continent–ocean boundary in the south. It is therefore possible that during this phase, which led to the complete rupture of the continental lithosphere, a strong lateral thermal gradient and a pronounced topography of the lithosphere/asthenosphere boundary may have been created due to a

change from a wide rift to a narrow rift, thereby causing strong secondary convection cells in the asthenosphere centred beneath and along the shoulders of the present continent–ocean boundary.

We therefore speculate that secondary mantle convection may have been responsible for a number of anomalous features of the rift–drift transition in the Taiwan region. These include (Fig. 20b and c) (1) Oligocene dynamic uplift of the rift flanks, (2) vigorous magmatism producing excess amounts of both extrusive and underplated igneous bodies adjacent to the continent–ocean boundary, (3) dike intrusions accompanying underplating in the outer margin, (4) thermal metamorphism in the outer margin and (5) rapid subsidence in the entire margin as the convection cell decays. In addition, the convection may also induce local rifting in the outer margin following the Oligocene uplift event. Local rifting may have also been assisted by a lateral pressure gradient caused by the preceding crustal uplift. This is similar to the case of 'active' continental rifting, which is preceded by a convecting mantle plume (e.g. Bott & Kusznir, 1979). As the effects of secondary convection decayed in the Taiwan margin, 'normal' thermal subsidence prevailed in the entire region (Fig. 20d).

Another anomalous feature is a phase of renewed postbreakup extension in the interval ∼ 12.5–6.5 Ma that occurred especially on the outer part of the margin (Fig. 20e). We speculate that recommenced sub-lithospheric convection cells may explain the renewed extension as well as other more or less coeval features: (1) An episode of diffusive intraplate volcanism (< 16 Ma) that followed the cessation of seafloor spreading in the South China Sea at ∼ 16 Ma (Briais *et al.*, 1993), affecting large parts of the continental margin of the South China Sea and intruding oceanic basement and relict continental fragments (Tu *et al.*, 1992; Chung *et al.*, 1994; Hoang *et al.*, 1996). The early stage of this volcanism is correlated to the Chiaopanshan volcanic episode (∼ 13–7.1 Ma) in the Taiwan region. (2) A < 12 Ma thermal metamorphism (Lan *et al.*, 1990) recorded in the Mesozoic basement of the Backbone Range.

CONCLUSIONS

West Taiwan basins have evolved from a rift setting through a post-breakup setting into a foreland basin. The temporal and spatial variability for this tectonic development has been constrained using an extensive subsurface data set. This analysis reveals the following:

1 Rifting (∼ 58–37 Ma): Lithospheric extension occurred simultaneously in discrete rift belts. These belts form a > 200-km-wide rift zone and are associated with a stretching factor, β, in the range ∼ 1.4–1.6. A nonmarine to marine, upper Palaeocene–middle Eocene syn-rift succession ponded in a series of fault-bounded rift grabens. These rift centres, if preserved, include the Nanjihtao, Penghu and Taihsi Basins. The Palaeogene syn-rift succession, now exposed in the Backbone and Hsuehshan Ranges

in Taiwan, represents the sediment deposited in the outer part of the margin.

2 Rift–drift transition (~ 37–30 Ma): As rifting progressed, the focus of rifting became concentrated at the present-day ocean–continent boundary off southern Taiwan, ~ 37 Ma, which led to continental rupture and initial seafloor spreading at ~ 30 Ma. The intense rifting during the rift–drift transition (~ 37–30 Ma) may have induced a transient, small-scale mantle convection beneath the rift. The immediate effects for the convection were (1) crustal uplift and erosion of the previously rifted margin (Oligocene uplift), (2) mafic dike intrusions (Jahn *et al.*, 1986; Juang & Bellon, 1986) accompanied by a phase of thermal metamorphism (Jahn *et al.*, 1986; Lan *et al.*, 1990) in the outer part of the previously rifted margin, and (3) vigorous magmatism that emplaced extrusive igneous bodies (cf. Sibuet *et al.*, 2002) and underplated igneous rocks (cf. Nissen *et al.*, 1995a, b) near the continent–ocean boundary. The Oligocene uplift and erosion (~ 37–30 Ma) led to the development of a pronounced Oligocene breakup unconformity. The large amount of erosion (up to 4500 m in the outer margin) partly eroded or completely overprinted the previous rift structures, especially in the outer margin where pronounced uplift/erosion occurred.

3 Post-breakup (~ 30–6.5 Ma): The Oligocene uplift was followed by rapid, early post-breakup subsidence (~ 30–18 Ma) possibly as the inferred induced convection abated following initial seafloor spreading. Rapid subsidence of the inner margin is interpreted as thermally controlled subsidence as evidenced by a lack of significant fault activities and a 'steer's head' basin geometry that shows younger sediments progressively onlapping onto the basin margin along the breakup unconformity. Rapid subsidence of the outer margin, however, was accompanied by normal faulting during the interval ~ 30–21 Ma and is interpreted as the initial subsidence associated with a new phase of rifting. This rifting event ($\beta \sim 1.5$) formed the Tainan Basin on top of the deeply eroded Mesozoic basement. During the interval ~ 21–12.5 Ma, the entire margin experienced broad thermal subsidence. It was not until ~ 12.5 Ma that rifting resumed, being especially active in the outer margin ($\beta \sim 1.1$). The ~ 12.5–6.5 Ma renewed extension in the outer margin created a major rift centre, the Northern Depression of the Tainan Basin, which was bordered by two rift flanks in the north and south, respectively (i.e. the Penghu Platform and the Central Uplift Zone of the Tainan Basin). Rifting ceased at ~ 6.5 Ma due to the orogeny caused by the over-riding of the Luzon volcanic arc.

4 Foreland basin development (~ 6.5–0 Ma): The Taiwan orogeny has created a foreland basin by loading and flexing the underlying rifted margin. The foreland flexure inherited the mechanical and thermal properties of the underlying rifted margin, thereby dividing the foreland flexure into north and south segments. The north segment developed on a lithosphere where the major rift/thermal event occurred ~ 58–30 Ma, and this segment shows minor normal faulting related to lithospheric deflection. In contrast, the south segment developed on top of the lithosphere,

where it experienced two more recent rift/thermal events during ~ 30–21 and ~ 12.5–6.5 Ma. The basal foreland surface of the south segment is highly faulted, especially along the previous northern rifted-flank, thereby creating a deeper foreland flexure that trends obliquely to the strike of the orogen.

ACKNOWLEDGEMENTS

REFERENCES

ATHY, L.F. (1930) Density, porosity and compaction of sedimentary rocks. *AAPG Bull.*, **14**, 1–24.

AUDET, D.M. (1995) Modelling of porosity evolution and mechanical compaction of calcareous sediments. *Sedimentology*, **42**, 355–373.

AUDET, D.M. (1996) Compaction and overpressuring in Pleistocene sediments on the Louisiana Shelf, Gulf of Mexico. *Mar. Pet. Geol.*, **13**, 467–474.

BOTT, M.H.P. & KUSZNIR, N. (1979) Stress distributions associated with compensated plateau uplift structures with application to the continental splitting mechanism. *Geophys. J. R. Astron. Soc.*, **56**, 451–459.

BOUTILIER, R.R. & KEEN, C.E. (1999) Small-scale convection and divergent plate boundaries. *J. Geophys. Res.*, **104**, 7389–7403.

BRIAIS, A., PATRIAT, P. & TAPPONNIER, P. (1993) Updated interpretation of magnetic-anomalies and sea-floor spreading stages in the South China Sea – implications for the Tertiary tectonics of Southeast Asia. *J. Geophys. Res.*, **98**, 6299–6328.

BUCK, W.R. (1986) Small-scale convection induced by passive margin rifting: the cause of uplift of rift shoulders. *Earth Planet. Sci. Lett.*, **77**, 362–372.

BURLAND, J.B. (1990) On the compressibility and shear strength of natural clays. *Geotechnique*, **40**, 329–378.

CANDE, S.C. & KENT, D.V. (1995) Revised calibration of the geomagnetic polarity time scale for the Late Cretaceous and Cenozoic. *J. Geophys. Res.*, **100**, 6093–6095.

CHOW, J., CHEN, H.-M., CHANG, T.-Y., KUO, C.-L. & TSAI, S.-F. (1991) Preliminary study on hydrocarbon plays around Nanjihtao Basin, Taiwan Strait. *Petrol. Geol. Taiwan*, **26**, 45–56.

CHUNG, S.-L., SUN, S.-S., TU, K., CHEN, C.-H. & LEE, C.-Y. (1994) Late Cenozoic basaltic volcanism around the Taiwan Strait, SE China: product of lithosphere–asthenosphere interaction during continental extension. *Chem. Geol.*, **112**, 1–20.

COCHRAN, J.R. (1983) Effect of finite rifting times on the development of sedimentary basins. *Earth Planet. Sci. Lett.*, **66**, 289–302.

FALVEY, D.A. (1974) The development of continental margins in plate tectonic theory. *Austr. Petrol. Exploration Assoc. J.*, **14**, 95–106.

FUH, S.-C. (2000) Magnitude of Cenozoic erosion from mean sonic transit time, offshore Taiwan. *Mar. Pet. Geol.*, **17**, 1011–1028.

GROW, J.A., KLITGORD, K.D. & SCHLEE, J.S. (1988) Structure and evolution of Baltimore Canyon Trough. In: *The Atlantic Continental Margin: The Geology of North America*, Vols. I-2 (Ed. by R.E. Sheridan & J.A. Grow), pp. 269–290. Geological Society of America, Boulder, CO.

HADDAD, D. & WATTS, A.B. (1999) Subsidence history, gravity anomalies, and flexure of the northeast Australian margin in Papua New Guinea. *Tectonics*, **18**, 827–842.

HAQ, B.U., HARDENBOL, J. & VAIL, P.R. (1987) Chronology of fluctuating sea levels since the Triassic. *Science*, **235**, 1156–1167.

HO, C.-S. (1986) *An Introduction to the Geology of Taiwan: Explanatory Text of the Geologic Map of Taiwan*, 2nd edn. Central Geological Survey, Taipei, Taiwan.

HOANG, N., FLOWER, M.F.J. & CARLSON, R.W. (1996) Major, trace element, and isotopic compositions of Vietnamese basalts: interaction of hydrous EM1-rich asthenosphere with thinned Eurasian lithosphere. *Geoch. Cosmoch. Acta*, **60**, 4329–4351.

HOLBROOK, W.S. & KELEMEN, P.B. (1993) Large igneous province on the U.S. Atlantic margin and implications for magmatism during continental breakup. *Nature*, **364**, 433–436.

HOLLOWAY, N.H. (1982) North Palawan Block, Philippines – its relation to the Asian mainland and role in evolution of South China Sea. *AAPG Bull.*, **66**, 1355–1383.

HSIAO, P.-T., HU, C.-C., LIN, K.A., HSU, S.-H., FUH, S.-C., CHANG, T.-Y., HSIUAN, T.-H., SHEEN, H.-C., KUO, C.-L. & LEE, C.-J. (1991) Hydrocarbon potential evaluation of the Penghu Basin. *Petrol. Geol. Taiwan*, **26**, 215–229 (in Chinese).

HSU, S.-K., LIU, C.-S., SHYU, C.-T., LIU, S.-Y., SIBUET, J.-C., LALLEMAND, S., WANG, C.-S. & REED, D. (1998) New gravity and magnetic anomaly maps in the Taiwan–Luzon region and their preliminary interpretation. *Terrestr. Atmosph. Oceanic Sci.*, **9**, 509–532.

HUANG, S.-T., CHEN, R.-C. & CHI, W.-R. (1993) Inversion tectonics and evolution of the northern Taihsi Basin, Taiwan. *Petrol. Geol. Taiwan*, **28**, 15–46.

HUANG, T.-C. (1978) Calcareous nannofossils of the subsurface pre-Miocene rocks from the Peikang Basement High and adjacent areas in western central Taiwan (Part I: Cretaceous). *Petrol. Geol. Taiwan*, **15**, 49–87.

HUANG, T.-C. (1980a) Calcareous nannofossils from the slate terrane west of Yakou, Southern Cross-Island Highway. *Petrol. Geol. Taiwan*, **17**, 59–74.

HUANG, T.-C. (1980b) Oligocene to Pleistocene calcareous nannofossil biostratigraphy of the Hsuehshan Range and Western Foothills in Taiwan. *Geol. Palaeontol. Southeast Asia*, **21**, 191–210.

HUANG, T.-C. (1982) Tertiary calcareous nannofossil stratigraphy and sedimentation cycles in Taiwan. In: *Proceedings of the Second ASCOPE Conference and Exhibition* (Ed. by A. Salivar-Sali), pp. 837–886. Manila, Philippines.

HUANG, T.-C. & CHI, W.-R. (1979) Calcareous nannofossils of the subsurface pre-Miocene rocks from the Peikang Basement High and adjacent areas in western central Taiwan (Part II: Palaeocene). *Petrol. Geol. Taiwan*, **16**, 95–129.

HUBBARD, R.J. (1988) Age and significance of sequence boundaries on Jurassic and Early Cretaceous rifted continental margins. *AAPG Bull.*, **72**, 49–72.

HUBBARD, R.J., PAPE, J. & ROBERTS, D.G. (1985) Depositional sequence mapping as a technique to establish tectonic and stratigraphic framework and evaluate hydrocarbon potential on a passive continental margin. In: *Seismic Stratigraphy II: An Integrated Approach* (Ed. by O.R. Berg & D.G. Woolverton), *AAPG Memoir*, **39**, 79–91.

ISSLER, D.R. (1992) A new approach to shale compaction and stratigraphic restoration, Beaufort–Mackenzie Basin and Mackenzie Corridor, northern Canada. *AAPG Bull.*, **76**, 1170–1189.

JAHN, B.-M., MARTINEAU, F., PEUCAT, J.J. & CORNICHET, J. (1986) Geochronology of the Tananao Schist Complex, Taiwan, and its regional tectonic significance. *Tectonophysics*, **125**, 103–124.

JUANG, W.-S. (1996) Geochronology and geochemistry of basalts in the Western Foothills, Taiwan. *Bull. Natl. Museum Nat. Sci.*, **7**, 45–98.

JUANG, W.-S. & BELLON, H. (1986) Potassium–argon ages of the Tananao Schist in Taiwan. *Mem. Geol. Soc. China*, **7**, 405–416.

KEEN, C.E. (1985) The dynamics of rifting: deformation of the lithosphere by active and passive driving forces. *Geophys. J. R. Astron. Soc.*, **80**, 95–120.

KEEN, C.E. & POTTER, D.P. (1995) The transition from a volcanic to a nonvolcanic rifted margin off eastern Canada. *Tectonics*, **14**, 359–371.

KELEMEN, P.B. & HOLBROOK, W.S. (1995) Origin of thick, high-velocity igneous crust along the US east coast margin. *J. Geophys. Res.*, **100**, 10077–10094.

LAN, C.-Y., LEE, T. & WANG-LEE, C.M. (1990) The Rb–Sr isotopic record in Taiwan gneisses and its tectonic implication. *Tectonophysics*, **183**, 129–143.

LEE, C.-Y., CHUNG, S.-L., CHEN, C.-H. & HSIEH, Y.-L. (1993a) Mafic granulite xenoliths from Penghu Islands: evidence for basic lower crust in SE China continental margin. *J. Geol. Soc.-China*, **36**, 351–379.

LEE, T.-Y. & LAWVER, L.A. (1992) Tectonic evolution of the South China Sea region. *J. Geol Soc. China*, **35**, 353–388.

LEE, T.-Y. & LAWVER, L.A. (1994) Cenozoic plate reconstruction of the South China Sea region. *Tectonophysics*, **235**, 149–180.

LEE, T.-Y., TANG, C.-H., TING, J.-S. & HSU, Y.-Y. (1993b) Sequence stratigraphy of the Tainan Basin, offshore southwestern Taiwan. *Petrol. Geol. Taiwan*, **28**, 119–158.

LIN, A.T. (2001) Cenozoic stratigraphy and tectonic development of the West Taiwan Basins. PhD Thesis, University of Oxford, Oxford, UK, 253pp.

LIN, A.T. & WATTS, A.B. (2002) Origin of the West Taiwan Basin by orogenic loading and flexure of a rifted continental margin. *J. Geophys. Res.*, **107**, ETG2-1–2-19.

LO, C.-H., CHUNG, S.-L., LEE, T.-Y., WANG, K.-L. & WU, C.-T. (2000) Cenozoic magmatism and rifted basin evolution around the Taiwan Strait, SE China continental margin. *Eos Trans. AGU*, **81**, 1111.

LO, C.-H. & YUI, T.-F. (1996) $^{40}Ar/^{39}Ar$ dating of high-pressure rocks in the Tananao basement complex, Taiwan. *J. Geol. Soc. China*, **39**, 13–30.

LUDMANN, T. & WONG, H.K. (1999) Neotectonic regime on the passive continental margin of the northern South China Sea. *Tectonophysics*, **311**, 113–138.

MARTINEZ, F., TAYLOR, B. & GOODLIFFE, A. (1999) Contrasting styles of seafloor spreading in the Woodlark Basin: indications of rift-induced secondary mantle convection. *J. Geophys. Res.*, **104**, 12909–12926.

MILLER, K.G., MOUNTAIN, G.S., BROWNING, J.V., KOMINZ, M., SUGARMAN, P.J., CHRISTIEBLICK, N., KATZ, M.E. & WRIGHT,

J.D. (1998) Cenozoic global sea level, sequences, and the New Jersey transect: results from coastal plain and continental slope drilling. *Rev. Geophys.*, **36**, 569–601.

MILLER, K.G., MOUNTAIN, G.S. & TUCHOLKE, B.E. (1985) Oligocene glacio-eustasy and erosion on the margins of the North Atlantic. *Geology*, **13**, 1–13.

MUTTER, J.C., BUCK, W.R. & ZEHNDER, C.M. (1988) Convective partial melting, I: a model for formation of thick basaltic sequences during the initiation of spreading. *J. Geophys. Res.*, **93**, 1031–1048.

NISSEN, S.S., HAYES, D.E., BUHL, P., DIEBOLD, J., YAO, B., ZENG, W. & CHEN, Y. (1995a) Deep penetration seismic soundings across the northern margin of the South China Sea. *J. Geophys. Res.*, **100**, 22407–22433.

NISSEN, S.S., HAYES, D.E., YAO, B., ZENG, W., CHEN, Y. & NU, X. (1995b) Gravity, heat flow, and seismic constraints on the processes of crustal extension – northern margin of the South China Sea. *J. Geophys. Res.*, **100**, 22447–22483.

PARASNIS, D.S. (1960) The compaction of sediments and its bearing on some geophysical problems. *Geophys. J. R. Astron. Soc.*, **3**, 1–28.

RAIGA-CLEMENCEAU, J., MARTIN, J.P. & NICOLETIS, S. (1988) The concept of acoustic formation factor for more accurate porosity determination from sonic transit time data. *Log Analyst*, **29**, 54–60.

SHEN, H.-C., HUANG, S.-T., TANG, C.-H. & HSU, Y.-Y. (1996) Geometrical characteristics of structural inversion on the offshore of Miaoli, Taiwan. *Petrol. Geol. Taiwan*, **30**, 79–110.

SIBUET, J.-C., HSU, S.-K., LE PICHON, X., LE FORMAL, J.-P., REED, D., MOORE, G. & LIU, C.-S. (2002) East Asia plate tectonics since 15 Ma: constraints from the Taiwan region. *Tectonophysics*, **344**, 103–134.

STECKLER, M.S., FEINSTEIN, S., KOHN, B.P., LAVIER, L.L. & EYAL, M. (1998) Pattern of mantle thinning from subsidence and heat flow measurements in the Gulf of Suez; evidence for the rotation of Sinai and along-strike flow from the Red Sea. *Tectonics*, **17**, 903–920.

STECKLER, M.S. & WATTS, A.B. (1978) Subsidence of the Atlantic-type continental margin off New York. *Earth Planet. Sci. Lett.*, **41**, 1–13.

SUN, S.-C. (1982) The Tertiary basins of offshore Taiwan. In: *Proceedings of the Second ASCOPE Conference and Exhibition* (Ed. by A. Salivar-Sali), pp. 125–135. Manila, Philippines.

SUPPE, J. (1980) A retrodeformable cross section of northern Taiwan. *Proc. Geol. Soc. China*, **23**, 46–55.

TANG, C.-H. (1977) Late Miocene erosional unconformity on the subsurface Peikang high beneath the Chiayi–Yunlin coastal plain, Taiwan. *Mem. Geol. Soc. China*, **2**, 155–167.

TAYLOR, B. & HAYES, D.E. (1980) The tectonic evolution of the South China Basin. In: *The Tectonic and Geologic Evolution of Southeast Asian Seas and Islands* (Ed. by D.E. Hayes), *AGU Geophysical Monograph*, **23**, 89–104.

TAYLOR, B. & HAYES, D.E. (1983) Origin and history of the South China Sea. In: *The Tectonic and Geologic Evolution of Southeast Asian Seas and Islands, Part 2* (Ed. by D.E. Hayes), *AGU Monograph*, **27**, 23–56.

TENG, L.S. (1990) Geotectonic evolution of late Cenozoic arc–continent collision in Taiwan. *Tectonophysics*, **183**, 57–76.

TENG, L.S., WANG, Y., TANG, C.-H., HUANG, C.-Y., HUANG, T.-C., YU, M.-S. & KE, A. (1991) Tectonic aspects of the Paleogene depositional basin of northern Taiwan. *Proc. Geol. Soc. China*, **34**, 313–336.

TU, K., FLOWER, M.F.J., CARLSON, R.W., ZHANG, M. & XIE, G.H. (1992) Magmatism in the South China Basin, 1. Isotopic and trace element evidence for an endogenous Dupal mantle component. *Chem. Geol.*, **97**, 47–63.

TZENG, J., UANG, Y.-C., HSU, Y.-Y. & TENG, L.S. (1996) Seismic stratigraphy of the Tainan Basin. *Petrol. Geol. Taiwan*, **30**, 281–307 (in Chinese).

VAIL, P.R., MITCHUM, R.M. Jr, TODD, R.G., WIDMIER, J.M., THOMPSON, S. III, SANGREE, J.B., BUBB, J.N. & HATLEILID, W.G. (1977) Seismic stratigraphy and global changes of sea level. In: *Seismic Stratigraphy – Applications to Hydrocarbon Exploration* (Ed. by C.E. Payton), *AAPG Memoir*, **26**, 49–212.

WATTS, A.B. (1992) The effective elastic thickness of the lithosphere and the evolution of foreland basins. *Basin Res.*, **4**, 169–178.

WATTS, A.B., KARNER, G.D. & STECKLER, M.S. (1982) Lithospheric flexure and the evolution of sedimentary basins. In: *The Evolution of Sedimentary Basins* (Ed. by P. Kent, M.H.P. Bott, D.P. McKenzie & C.A. Williams), *Phil. Trans. Roy. Soc. London*, **305A**, 249–281.

WATTS, A.B. & RYAN, W.B.F. (1976) Flexure of the lithosphere and continental margin basins. *Tectonophysics*, **36**, 25–44.

WATTS, A.B. & STECKLER, M.S. (1979) Subsidence and eustasy at the continental margin of eastern North America. In: *Deep Drilling Results in the Atlantic Ocean: Continental Margins and Palaeoenvironments, Volume 3 of Maurice Ewing Series* (Ed. by M. Talwani, W. Hay & W. B. F. Ryan), pp. 218–234. AGU.

WESSEL, P. & SMITH, W.H.F. (1995) New version of the Generic Mapping Tools released. *Eos Trans. AGU*, **76**, 329.

WHITE, R.S. & MCKENZIE, D.P. (1989) Magmatism at rift zones: the generation of volcanic continental margins and flood basalts. *J. Geophys. Res.*, **94**, 7685–7729.

WHITE, R.S., WESTBROOK, G.K., BOWEN, A.N., FOWLER, S.R., SPENCE, G.D., PRESCOTT, C., BARTON, P.J., JOPPEN, M., MORGAN, J. & BOTT, M.H.P. (1987) Hatton Bank (northwest U.K.) continental margin structure. *Geophys. J. R. Astron. Soc.*, **89**, 265–272.

YANG, K.-M., TING, H.-H. & YUAN, J. (1991) Structural styles and tectonic modes of Neogene extensional tectonics in southwestern Taiwan: implication for hydrocarbon exploration. *Petrol. Geol. Taiwan*, **26**, 1–31.

YIELDING, G. (1990) Footwall uplift associated with Late Jurassic normal faulting in the northern North Sea. *J. Geol. Soc. London*, **147**, 219–222.

YU, H.-S. & CHOU, Y.-W. (2001) Characteristics and development of the flexural forebulge and basal unconformity of Western Taiwan Foreland Basin. *Tectonophysics*, **333**, 277–291.

ZEHNDER, C.M., MUTTER, J.C. & BUHL, P. (1990) Deep seismic and geochemical constraints on the nature of rift-induced magmatism during breakup of the North Atlantic. *Tectonophysics*, **173**, 545–565.

ZHOU, D., RU, K. & CHEN, H.Z. (1995) Kinematics of Cenozoic extension on the South China Sea continental margin and its implications for the tectonic evolution of the region. *Tectonophysics*, **251**, 161–177.